Modeling animal movement with directional persistence and attractive points

Submitted to the Annals of Applied Statistics

MODELING ANIMAL MOVEMENT WITH DIRECTIONAL PERSISTENCE AND ATTRACTIVE POINTS

By Gianluca Mastrantonio,

Department of Mathematical Sciences, Politecnico di Torino, gianluca.mastrantonio@polito.it

GPS technology is currently easily accessible to researchers, and many animal movement datasets are available. Two of the main features that a model which describes an animal's path can possess are directional persistence and attraction to a point in space. In this work, we propose a new approach that can have both characteristics.

Our proposal is a hidden Markov model with a new emission distribution. The emission distribution models the two aforementioned characteristics, while the latent state of the hidden Markov model is needed to account for the behavioral modes. We show that the model is easy to implement in a Bayesian framework.

We estimate our proposal on the motivating data that represent GPS locations of a Maremma Sheepdog recorded in Australia. The obtained results are easily interpretable and we show that our proposal outperforms the main competitive model.

1. Introduction. The use of statistical models to understand the movement of animals has become increasingly popular. The data of such models are generally in the form of a time series of 2-dimensional spatial locations, recorded using a GPS device attached to the animal, with a time-interval between observations programmed by the researcher (Cagnacci *et al.*, 2010). These data are often called "trajectory tracking data", and they allow features of an animal's movement, such as habitat selection (Hebblewhite and Merrill, 2008), spatio-temporal patterns (Morales *et al.*, 2004; Fryxell *et al.*, 2008; Nathan *et al.*, 2008; Frair *et al.*, 2010) and animal behavior (Merrill and David Mech, 2000; Anderson and Lindzey, 2003), to be investigated; for a detailed review, the reader may refer to Hooten *et al.* (2017). These approaches can be grouped into three main categories: point processes (Johnson *et al.*, 2013; Brost *et al.*, 2015), continuous-time dynamic models (CTM) (Blackwell, 1997; Johnson *et al.*, 2008; Fleming *et al.*, 2014; Hanks *et al.*, 2015; Buderman *et al.*, 2018a,b) and discrete-time dynamic models (DTM) (Morales *et al.*, 2004; Jonsen *et al.*, 2005; McClintock *et al.*, 2012). Animal movement is a continuous process, but it is generally easier to interpret and analyze a DTM if the time-interval between observations is fixed (Codling and Hill, 2005; Patterson *et al.*, 2017). For a discussion on the differences between and similarities of these approaches, the reader may refer to McClintock *et al.* (2014).

Most of the proposed models, in both continuous- and discrete-time frameworks, are based on biased random walks (BRWs) and correlated random walks (CRWs). In a BRW, the animal is attracted to a specific spatial location, called *center-of-attraction* (see, for example, Blackwell, 1997; Dunn and Gipson, 1977), which can be used to model a tendency to move toward a patch of space (McClintock *et al.*, 2012) or the home range (Christ *et al.*, 2008). On the other hand, in a CRW, the movement direction, at a given time, depends on the previous one; this property is called directional persistence. A CRW is often expressed using *movement-metrics*, e.g., *step-length* and *turning-angle* or

Keywords and phrases: Maremma Sheepdog, Step-Length, Turning-Angle, CRW, BRW.

step-length and *bearing-angle*, which are proxies of the speed and the direction measured between consecutive locations. These models are often referred to as *step and turn* models (Parton and Blackwell, 2017). Independence between the movement-metrics is usually assumed, see, for example, Morales and Ellner (2002) and Patterson *et al.* (2017), and they are rarely dependent (Mastrantonio, 2018; Mastrantonio *et al.*, 2019). The correlation between locations is a necessary but not sufficient condition for a model to be a CRW, e.g., a two-dimensional AR(1) model is a BRW, but not a CRW, since there is no correlation between consecutive turning-angles or bearing-angles. Most of the proposed models have only a BRW or CRW characteristic, but there are some approaches, called biased and correlated random walks (BCRWs), which have both (Schultz and Crone, 2001; Fortin *et al.*, 2005; Codling *et al.*, 2008; McClintock *et al.*, 2012). In order to be able to detect changes in the behavior of an animal (behavioral modes), the data are generally modeled conditionally to a latent discrete state that describes the behavior assumed by the animal at a given time (Patterson *et al.*, 2008). Switching between behavioral modes is often assumed to be temporally structured, and if it follows a Markov process the model is said to be a hidden Markov model (HMM) (Michelot *et al.*, 2016; Langrock *et al.*, 2012). In the HMM context, the distribution of the data is called emission distribution (Volant *et al.*, 2014).

In this work, we propose an HMM with a new emission distribution which is called *step and turn with an attractive point (STAP)*; the STAP belongs to the BCRW family. We define the STAP by combining a CRW and a BRW. For the CRW part, we envision the step-length and turning-angle as the polar-coordinate representation of Cartesian coordinates. The Cartesian coordinates are assumed to be normally distributed, which induces a conditional normal distribution on the spatial locations. We use an AR(1) model with a normal conditional distribution for the BRW part. We can thus combine the two by introducing a parameter $\rho \in [0, 1]$, which defines a conditional normal distribution with a mean and covariance matrix that reduces to those of the BRW when $\rho = 0$ and to those of the CRW if $\rho = 1$, with a bias toward the center-of-attraction and a directional persistence for any value in between. The distribution we define for ρ allows us to detect whether a behavior follows BRW, CRW or BCRW dynamics. Our HMM is formalized in a Bayesian setting, using the sticky hierarchical Dirichlet process HMM (sHDP-HMM) of Fox *et al.* (2011). The sHDP-HMM is a general framework that is used to define an HMM with any emission distribution, and it is based on the Dirichlet process (DP). We indicate as STAP-HMM the sHDP-HMM with the STAP as emission distribution. The use of the DP and of the distribution we define for ρ, allows us to treat the number of behaviors as a random variable, which can then be estimated during the model fitting, and to select the behavior-type without the need to resort to information criteria or a trans-dimensional Markov chain Monte Carlo algorithm (MCMC), such as the reversible jump MCMC (RJMCMC), which involves challenges in its implementation (Hastie and Green, 2012).

Although other BCRWs model the circular mean of the turning- or bearing-angle to induce attraction and directional persistence (Fortin *et al.*, 2005; Barton *et al.*, 2009; Rivest *et al.*, 2016), we approach the problem from a different point of view by modeling the movement path with a normal distribution, and hence inducing attraction and directional persistence on the bi-dimensional movement directly. This allows not only a straightforward inference but, as a by-product, to have a projected-normal distribution for the bearing- and turning-angle, which is, to-date, the most flexible distribution for circular data (Mastrantonio *et al.*, 2015). On the other hand, competitive models, i.e., HMMs with a BCRW emission distribution, use unimodal and symmetrical circular distributions for interpretability and easiness of implementation (e.g., the von-Mises,

wrapped Normal or wrapped Cauchy), thereby limiting the flexibility of the model. Most BCRW models can be formalized in the general framework proposed by McClintock *et al.* (2012), which we consider as our main competitive model.

We use our proposal to model the trajectory tracking data of a Maremma Sheepdog. These dogs have been used for centuries in Europe and Asia to protect livestock from predators, but only recently in Australia (Gehring *et al.*, 2017; van Bommel and Johnson, 2016). They generally work with the shepherd to keep the stock together but, due to the size of the properties, this is not always possible in Australia. Since an owner is often unaware of his/her dog's behavior, it is of interest to understand and characterize such behavior. We analyze a dataset taken from the movebank repository (`www.movebank.org`) in which the spatial locations of a dog, used to protect livestock in a property in Australia, are recorded using a GPS device (van and Johnson, 2014; van Bommel and Johnson, 2014). We also show that our proposal outperforms the model of McClintock *et al.* (2012) in terms of "deviance information criterion" (DIC) (Celeux *et al.*, 2006) and "integrated classification likelihood" (ICL) (Biernacki *et al.*, 2000).

The paper is organized as follows. We formalize the model in Section 2, by introducing the CRW (Section 2.2), the BRW (Section 2.3), then the STAP models (Section 2.4) and finally the STAP-HMM (Section 2.5). In Section 2.6, we show the similarities and differences between our proposal and the general framework of McClintock *et al.* (2012). The conclusive remarks are presented in 4. In the Appendix, we show how to implement the MCMC algorithm (Appendix A), some simulated examples (Appendix B), a description of the McClintock *et al.* (2012) proposal (Appendix C), how the turning-angle distribution changes if we change the time-interval between the recorded coordinates (Appendix D), a sensitivity analysis of the sHDP-HMM hyper-parameter priors (Appendix E), simulated paths obtained with parameters estimated from the real data application (Appendix F), and the results of STAP-HMMs that are only able to estimate CRW or BRW behaviors (Appendix G).

2. Methods. We assume we have a time-series of spatial coordinates $\mathbf{s} = (\mathbf{s}_1, \ldots, \mathbf{s}_T)'$, with $\mathbf{s}_i = (s_{i,1}, s_{i,2}) \in \mathcal{D} \subset \mathbb{R}^2$, which represent the animal's path in a two-dimensional space. We assume there is no measurement error and the time-difference between consecutive observations is fixed. We consider coordinates $\mathbf{s}_{i+1}$ as the realization of a random variable with the following conditional distribution:

$$\mathbf{s}_{i+1}|\mathbf{s}_i, \mathbf{s}_{i-1}, \ldots, \mathbf{s}_1 \sim N(\mathbf{s}_i + \mathbf{M}_i, \mathbf{V}_i),\ i \in \{1, \ldots, T-1\}, \tag{1}$$

where $\mathbf{M}_i = (M_{i,1}, M_{i,2})' \in \mathbb{R}^2$ and $\mathbf{V}_i$ is a 2×2 covariance matrix. The vector $\mathbf{M}_i$ and the matrix $\mathbf{V}_i$ may depend on previous locations and other parameters, while $\mathbf{s}_1$ is known and fixed. The conditional set is composed of the entire past but, as we will show in Section 2.4, only the two previous locations are needed in our proposal, and $\mathbf{s}_0$ is therefore considered as a parameter that is able to define the conditional distribution of $\mathbf{s}_2$. Equation (1) models the path intuitively, since the animal moves at each time-point following a normal distribution, with the mean coordinates given by the previous location and parameter $\mathbf{M}_i$, while $\mathbf{V}_i$ measures the variability.

In Figure 1, it is possible to see how $\mathbf{M}_i$ and $\mathbf{V}_i$ are connected to the observed path, since the end-point of the arrow represents the mean value of the conditional distribution of $\mathbf{s}_{i+1}$ (which is $\mathbf{s}_i + \mathbf{M}_i$), while the ellipse is the set of points $\mathbf{s}^* \in \mathbb{R}^2$ that satisfy $(\mathbf{s}^* - \mathbf{s}_i - \mathbf{M}_i)'\mathbf{V}_i^{-1}(\mathbf{s}^* - \mathbf{s}_i - \mathbf{M}_i) = c$, where the value c is defined to ensure that the area $\mathcal{E} \in \mathbb{R}^2$ inside the ellipse contains 95% of the probability mass of the conditional distribution of $\mathbf{s}_{i+1}$, i.e.,

$$\int_{\mathbf{s} \in \mathcal{E}} (2\pi)^{-1} |\mathbf{V}_i|^{-\frac{1}{2}} \exp\left(-\frac{(\mathbf{s} - \mathbf{s}_i - \mathbf{M}_i)'\mathbf{V}_i^{-1}(\mathbf{s} - \mathbf{s}_i - \mathbf{M}_i)}{2} \right) d\mathbf{s} = 0.95. \tag{2}$$

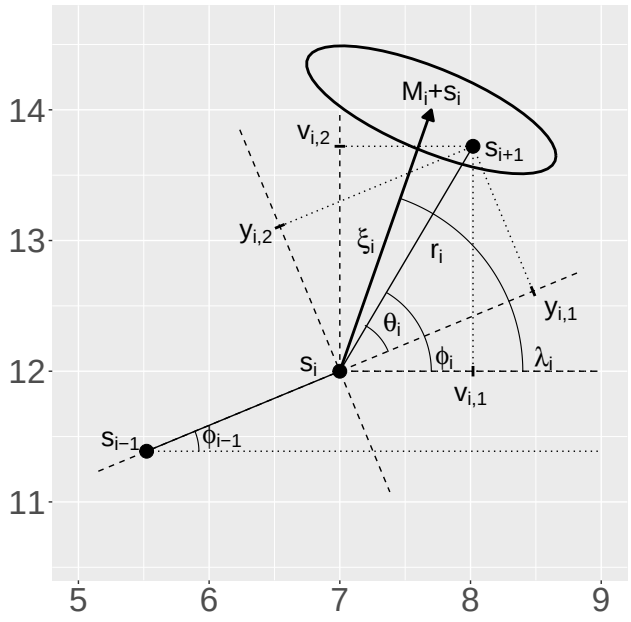

Fig 1: A graphical representation of the relations between the spatial locations, the movement-metrics and the displacement-coordinate. The arrow represents $\vec{\mathbf{F}}_i$, while the ellipse is an area containing 95% of the probability mass of the conditional distribution of $\mathbf{s}_{i+1}$, computed using (2).

It should be noted that the value of the conditional density of $\mathbf{s}_{i+1}$ is the same for all $\mathbf{s}^*$ on the ellipse, hence the ellipse is a contour of the normal density, and it can be used to represent and to infer the characteristics of the covariance matrix $\mathbf{V}_i$ (Friendly *et al.*, 2013). For example, let $x \in (-\pi/2, \pi/2]$ be the inclination angle of the major axis of the ellipse, then the correlation is >0 if $0 < x < \pi/2$, <0 if $-\pi/2 < x < 0$, and there is no correlation if $x = 0$ or $x = \pi/2$, i.e., the major axis of the ellipse is parallel to one of the two axes of the Euclidian reference system. If we indicate the largest values of the first and second Euclidean coordinate in $\mathcal{E}$ as x_1^* and x_2^*, respectively, the distances $x_1^* - s_{i,1} - M_{i,1}$ and $x_2^* - s_{i,2} - M_{i,2}$ are proxies of the two variances of $\mathbf{V}_i$. If the ellipse is a circle, there is no correlation and the two variances have the same value.

Parameter $\mathbf{M}_i$ can be used to introduce such movement features as directional persistence and a center-of-attraction. To describe these two features, we introduce the vector $\vec{\mathbf{F}}_i$, which is a vector with initial and terminal points $\mathbf{s}_i$ and $\mathbf{s}_i + \mathbf{M}_i$, respectively (see Figure 1), and it represents the expected movement between time i and $i+1$ since its initial position is the previous observed location $\mathbf{s}_i$, while the terminal point is equal to $\mathbb{E}(\mathbf{s}_{i+1}|\mathbf{s}_i) = \mathbf{s}_i + \mathbf{M}_i$. The length of $\vec{\mathbf{F}}_i$, ξ_i, is equal to

$$||(\mathbf{s}_i + \mathbf{M}_i) - \mathbf{s}_i||_2 = ||\mathbf{M}_i||_2,$$

while its direction, λ_i, is equal to

$$\text{atan}^*((s_{i,2} + M_{i,2}) - s_{i,2}, (s_{i,1} + M_{i,1}) - s_{i,1}) = \text{atan}^*(M_{i,2}, M_{i,1}) \in [-\pi, \pi),$$

where $\text{atan}^*(\cdot)$ is the two-argument tangent function (Jammalamadaka and Kozubowski, 2004), i.e., the direction and length of $\vec{\mathbf{F}}_i$ are equal to those of $\mathbf{M}_i$. We introduce the bearing-angle

$$\phi_i = \text{atan}^*(s_{i+1,2} - s_{i,2}, s_{i+1,1} - s_{i,1}). \tag{3}$$

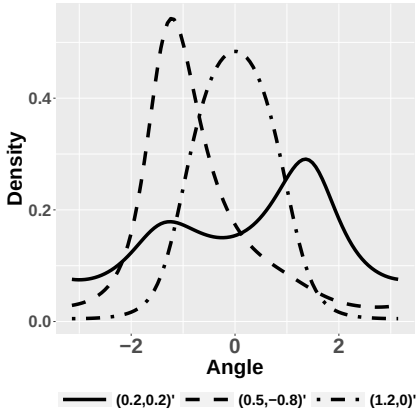

Fig 2: Representation of projected-normal densities based on a bivariate normal distribution with variances (0.5,1), 0 correlation and different mean vectors.

which measures the direction between locations $\mathbf{s}_i$ and $\mathbf{s}_{i+1}$. The distribution of ϕ_i, in a BRW, is independent of the previous bearing-angles and λ_i is equal to $\text{atan}^*(\mu_2 - s_{i,2}, \mu_1 - s_{i,1})$, which is the direction between the location in space $\boldsymbol{\mu} = (\mu_1, \mu_2)' \in \mathbb{R}^2$ and the previous observed location $\mathbf{s}_i$. In this case, the vector $\boldsymbol{\mu}$ is a parameter that is used to define $\mathbf{M}_i$. Since the expected movement at time $i+1$, measured by $\vec{\mathbf{F}}_i$, starts from $\mathbf{s}_i$ and points to $\boldsymbol{\mu}$, the latter is called the attractor, since it "attracts" the animal. The distribution of ϕ_i, in a CRW, depends on the previous bearing-angles (albeit generally only on the first one, ϕ_{i-1}), which means that the directions are correlated. This is often done by assuming that λ_i is a function of ϕ_{i-1}, see, for example, Mastrantonio *et al.* (2019). It should be noted that a CRW needs to be at least second-order Markovian since two previous locations are needed to compute ϕ_{i-1}. In both models, ξ_i is a measure of how far the mean value of the conditional distribution of $\mathbf{s}_{i+1}$ is from $\mathbf{s}_i$, and it can be considered a proxy of the expected bi-dimensional movement speed. Parameter ξ_i can be also used, in a BRW, to evaluate the strength of the attraction, see Section 2.3. As we will show in Sections 2.2 and 2.3, parameter $\mathbf{V}_i$, in our definition of a CRW and BRW, depends on the previous direction in the CRW, and is independent of the previous direction and the attractor in the BRW.

Models based on equation (1) with only one of the two aforementioned features, i.e., directional persistence or an attractive point, have already been proposed (see, for example, Christ *et al.* (2008) and Mastrantonio *et al.* (2019)), and one of the main contributions of this paper is that it allows both properties to be considered.

2.1. *Displacement-coordinates and movement-metrics.* In this section, we introduce different ways of parametrizing the movement path that are useful to understand and interpret our approach. The relations between these quantities are also depicted in Figure 1.

The path $\mathbf{s}$ can be described equivalently by using $\mathbf{s}_1$ and the displacement-coordinates $\mathbf{v} = (\mathbf{v}_1, \ldots, \mathbf{v}_{T-1})'$, where $\mathbf{v}_i = \mathbf{s}_{i+1} - \mathbf{s}_i$, since

$$\mathbf{s}_{i+1} = \mathbf{s}_1 + \sum_{l=1}^{i} \mathbf{v}_l, \ i \in \{1, \ldots, T-1\}. \tag{4}$$

Variable $\mathbf{v}_i$ represents the movement between time i and $i+1$ and, from equation (1), we can easily derive that

$$\mathbf{v}_i | \mathbf{v}_{i-1}, \ldots, \mathbf{v}_1 \sim N(\mathbf{M}_i, \mathbf{V}_i), \ i \in \{1, \ldots, T-1\}. \tag{5}$$

The coordinates $\mathbf{v}_i$ are useful to describe an attractive point, since we can evaluate how it changes with respect to the distance from the attractor. Vector $\mathbf{v}_i$ can be expressed in polar-coordinates using its magnitude $r_i = ||\mathbf{v}_i||_2$ and the bearing-angle ϕ_i which can be computed using equation (3) or the following:

$$\phi_i = \text{atan}^*(v_{i,2}, v_{i,1}).$$

The value of r_i is the animal speed, and ϕ_i measures the direction with respect to the "general" reference-system, where $\phi_i = 0$ indicates the East direction, and the sense of rotation is anticlockwise. In animal-movement literature r_i is known as the step-length.

We can define a new set of displacement-coordinates if we let the reference-system change at each time-point, and align the x-axis in the direction of the previous increment $\mathbf{s}_i - \mathbf{s}_{i-1}$ with origin on the coordinate $\mathbf{s}_i$. We introduce the rotation matrix

$$\mathbf{R}(\omega) = \begin{pmatrix} \cos(\omega) & -\sin(\omega) \\ \sin(\omega) & \cos(\omega) \end{pmatrix},$$

which is a matrix that can be used to perform a rotation in a 2-dimensional space, and we define the new displacement-coordinates as

$$\mathbf{y}_i = \mathbf{R}'(\phi_{i-1})\mathbf{v}_i = \mathbf{R}'(\phi_{i-1})(\mathbf{s}_{i+1} - \mathbf{s}_i), \tag{6}$$

which represent the projection of $\mathbf{v}_i$ onto the direction of the increment $\mathbf{s}_i - \mathbf{s}_{i-1}$ measured by the bearing-angle ϕ_{i-1}, see Figure 1. From (5) and (6), we obtain

$$\mathbf{y}_i|\mathbf{y}_{i-1}, \ldots, \mathbf{y}_1 \sim N(\mathbf{R}'(\phi_{i-1})\mathbf{M}_i, \mathbf{R}'(\phi_{i-1})\mathbf{V}_i\mathbf{R}(\phi_{i-1})),\ i \in \{1, \ldots, T-1\}, \tag{7}$$

where ϕ_0 is a parameter, since it is a function of the fixed coordinate $\mathbf{s}_1$ and parameter $\mathbf{s}_0$. The transformation (6) preserves the vector magnitude, which then results in $r_i = ||\mathbf{v}_i||_2 = ||\mathbf{y}_i||_2$. The polar-coordinate representation of $\mathbf{y}_i$ is the couple (θ_i, r_i) where

$$\theta_i = \text{atan}^*(y_{i,2}, y_{i,1}). \tag{8}$$

The angle θ_i is called turning-angle and it is related to the bearing angle through the relation

$$\theta_i = \phi_i - \phi_{i-1}, \tag{9}$$

which highlights how θ_i and $\mathbf{y}_i$ represent a change in direction between two consecutive time-points and they are therefore useful to describe and introduce directional persistence, see the next section.

The polar-coordinates (ϕ_i, r_i) and (θ_i, r_i) are called movement-metrics, and they are often modeled instead of the coordinates, especially in CRWs, but also in BCRWs (McClintock *et al.*, 2012). The distribution over the angular variable is generally assumed to be unimodal and symmetric (Michelot *et al.*, 2016; Patterson *et al.*, 2017), with a few exceptions (see, for example, Mastrantonio (2018)). On the other hand, since both $\mathbf{v}_i$ and $\mathbf{y}_i$ are normally distributed, the bearing- and turning-angle of our proposal are projected normal distributed (Mastrantonio *et al.*, 2016), which is one of the most flexible distributions for circular data, with a density that can be unimodal symmetric, asymmetric, bimodal or antipodal; some examples of projected normal densities are shown in Figure 2, and more details can be found in Wang and Gelfand (2013).

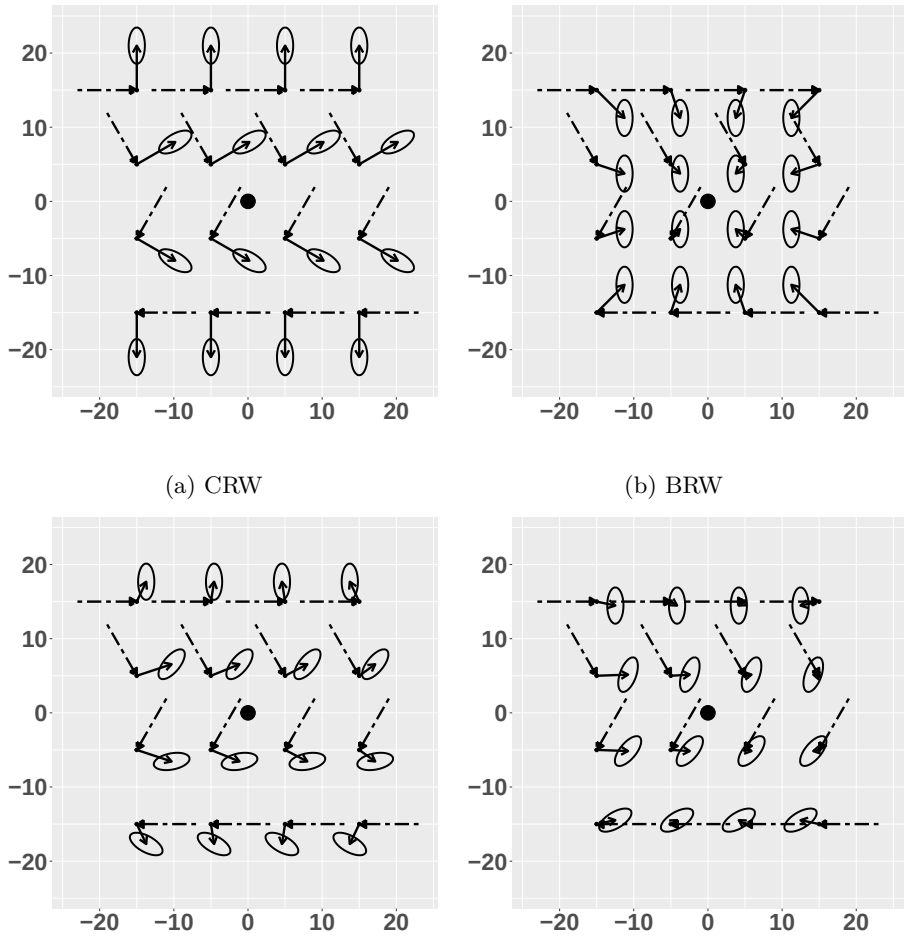

(a) CRW

(b) BRW

(c) BCRW with $\rho = 2/3$

(d) BCRW with $\rho = 1/3$

Fig 3: Graphical representation of the conditional distribution of $\mathbf{s}_{i+1}$ for different possible values of $\mathbf{s}_i$ and the previous directions. The dashed arrow represents the movement between $\mathbf{s}_{i-1}$ and $\mathbf{s}_i$. The solid arrow is $\vec{\mathbf{F}}_i$, while the ellipse is the area containing 95% of the probability mass of the conditional distribution of $\mathbf{s}_{i+1}$, computed using (2). In all the figures, $\boldsymbol{\mu} = (0,0)'$, $\boldsymbol{\eta} = (0,6)'$, $\tau = 0.25$, $\boldsymbol{\Sigma} = \begin{pmatrix} 0.2 & 0 \\ 0 & 1 \end{pmatrix}$, and the central dot is the location $\boldsymbol{\mu}$, which represents the attractor in the BRW and the BCRW.

2.2. *Correlated random walk.* To define the CRW, which is one of the two components needed as the base of our proposal, we model the displacement-coordinates $\mathbf{y}_i$ as

$$\mathbf{y}_i \sim N(\boldsymbol{\eta}, \boldsymbol{\Sigma}), \tag{10}$$

where $\boldsymbol{\eta} = (\eta_1, \eta_2)' \in \mathbb{R}^2$ is a vector of length 2 and $\boldsymbol{\Sigma}$ is a 2×2 covariance matrix. From equation (10), we can compute the following conditional distributions:

$$\mathbf{s}_{i+1} | \mathbf{s}_i, \mathbf{s}_{i-1} \sim N(\mathbf{s}_i + \mathbf{R}(\phi_{i-1})\boldsymbol{\eta}, \mathbf{R}(\phi_{i-1})\boldsymbol{\Sigma}\mathbf{R}'(\phi_{i-1})), \tag{11}$$

$$\mathbf{v}_i | \mathbf{v}_{i-1} \sim N(\mathbf{R}(\phi_{i-1})\boldsymbol{\eta}, \mathbf{R}(\phi_{i-1})\boldsymbol{\Sigma}\mathbf{R}'(\phi_{i-1})). \tag{12}$$

Since the bearing-angle ϕ_i is computed using $\mathbf{s}_i$ and $\mathbf{s}_{i-1}$, see equation (3), the path is second-order Markovian. The distribution (11) is in the form given by (1) with $\mathbf{M}_i = \mathbf{R}(\phi_{i-1})\boldsymbol{\eta}$ and $\mathbf{V}_i = \mathbf{R}(\phi_{i-1})\boldsymbol{\Sigma}\mathbf{R}'(\phi_{i-1})$. In this model, the parameters are $\boldsymbol{\eta}$, $\boldsymbol{\Sigma}$ and $\mathbf{s}_0$.

The angle λ_i, which is the direction of $\vec{\mathbf{F}}_i$, does not depend on the spatial location, but only on the bearing angle ϕ_{i-1} which rotates the parameter $\boldsymbol{\eta}$. In more detail, we have

$$\lambda_i = \phi_{i-1} + \text{atan}^*(\eta_2, \eta_1), \tag{13}$$

where $\text{atan}^*(\eta_2, \eta_1)$ is the direction of $\boldsymbol{\eta}$. Equation (13) shows that λ_i, the direction of the expected movement, is a rotation of the previous bearing-angle by an amount $\text{atan}^*(\eta_2, \eta_1)$, that is a function of $\boldsymbol{\eta}$. The value λ_i depends of the previous bearing-angle ϕ_{i-1}, and ϕ_i and ϕ_{i-1} are, therefore, correlated; this defines a CRW (see the beginning of Section 2). For example, if $\boldsymbol{\eta} = (1, 0)$ (i.e., $\text{atan}^*(\eta_2, \eta_1) = 0$), we obtain $\lambda_i = \phi_{i-1}$, if $\boldsymbol{\eta} = (0, 1)$ (i.e., $\text{atan}^*(\eta_2, \eta_1) = \pi/2$), we obtain $\lambda_i = \phi_{i-1} + \pi/2$, and $\lambda_i = \phi_{i-1} - \pi/2$ if $\boldsymbol{\eta} = (0, -1)$ (i.e., $\text{atan}^*(\eta_2, \eta_1) = -\pi/2$). The length of $\boldsymbol{\eta}$ is equal to ξ_i, since $||\mathbf{M}_i||_2 = ||\mathbf{R}(\phi_{i-1})\boldsymbol{\eta}||_2 = ||\boldsymbol{\eta}||_2$, and it represents the distance between $\mathbf{s}_i$ and $\mathbb{E}(\mathbf{s}_{i+1}|\mathbf{s}_i)$. It should be noted that the covariance matrix of $\mathbf{v}_i$ and $\mathbf{s}_{i+1}$ rotates according to the bearing-angle ϕ_{i-1}. The step-length and turning-angle, and variable $\mathbf{y}_i$, are i.i.d. and independent of the position in space and of the previous movement, while the parameters of the distribution of the bearing-angle and $\mathbf{v}_i$ change according to ϕ_{i-1} (see equation (12)).

In Figure 3 (a), we show the conditional distribution of $\mathbf{s}_{i+1}$ under different conditions, where all the features we described can easily be seen. Each vector $\vec{\mathbf{F}}_i$ (solid arrow) has the same length ($\xi_i = ||\boldsymbol{\eta}||_2 = 6$), regardless of the position in space (the tail of $\vec{\mathbf{F}}_i$) and the previous movement (dashed arrow). The value of λ_i depends on the previous direction, but the angle between the previous direction and $\vec{\mathbf{F}}_i$ is fixed and equal to $\text{atan}^*(\eta_2, \eta_1) = \pi/2$. The ellipse rotates with the bearing angle ϕ_{i-1}.

It should be noted that it is not possible to find a closed-form expression for the distribution of $\mathbf{s}_{i+l}|\mathbf{s}_i, \mathbf{s}_{i-1}$ if $l > 1$, for the proposed CRW. Hence, the CRW can be used if the time-interval is constant, since, even in the simple case in which there is no recorded observation for time $i + 1$, we are unable to compute the conditional density $\mathbf{s}_{i+2}|\mathbf{s}_i, \mathbf{s}_{i-1}$ ($l = 2$). Hence, in order to be able to compute the data likelihood in the MCMC algorithm, any missing data must be considered a further parameter and estimated during model fitting.

2.3. *Biased random walk.* We use a two-dimensional AR(1) model for the BRW component of our proposal

$$\mathbf{s}_{i+1}|\mathbf{s}_i \sim N(\mathbf{s}_i + \tau\,(\boldsymbol{\mu} - \mathbf{s}_i)\,, \boldsymbol{\Sigma}), \tag{14}$$

where $\boldsymbol{\mu}$ is a two-dimensional vector and $\tau \in (0, 1)$. The process is first-order Markovian and can be expressed as equation (1) by setting $\mathbf{M}_i = \tau\,(\boldsymbol{\mu} - \mathbf{s}_i)$ and $\mathbf{V}_i = \boldsymbol{\Sigma}$. The parameters, in this model, are $\boldsymbol{\mu}$, τ, and $\boldsymbol{\Sigma}$. The distributions of the displacement-coordinates are

$$\mathbf{v}_i|\mathbf{v}_{i-1}, \ldots, \mathbf{v}_1 \sim N(\tau\,(\boldsymbol{\mu} - \mathbf{s}_i)\,, \boldsymbol{\Sigma}), \tag{15}$$

$$\mathbf{y}_i|\mathbf{y}_{i-1}, \ldots, \mathbf{y}_1 \sim N(\mathbf{R}'(\phi_{i-1})\tau\,(\boldsymbol{\mu} - \mathbf{s}_i)\,, \mathbf{R}'(\phi_{i-1})\boldsymbol{\Sigma}\mathbf{R}(\phi_{i-1})), \tag{16}$$

where $\mathbf{s}_i$ is a function of the previous displacement-coordinates through equations (4) and (6). The direction of $\vec{\mathbf{F}}_i$ is equal to

$$\lambda_i = \text{atan}^*(\tau(\mu_2 - s_{i,2}), \tau(\mu_1 - s_{i,1})) = \text{atan}^*(\mu_2 - s_{i,2}, \mu_1 - s_{i,1}),$$

where it is clear that $\vec{\mathbf{F}}_i$ points to the parameter (or point in space) $\boldsymbol{\mu}$, and the former is therefore the spatial-attractor, i.e., we expect the movement to be in the direction of $\boldsymbol{\mu}$. Since the path described by equation (16) is first-order Markovian, the distribution of ϕ_i is independent of the previous bearing angles and only depends on the spatial coordinate $\mathbf{s}_i$ and $\boldsymbol{\mu}$, see equations (14) and (15). Hence, the two-dimensional AR(1) model is a BRW (see the beginning of Section 2). The length of $\vec{\mathbf{F}}_i$, ξ_i, is equal to $\tau||\boldsymbol{\mu}-\mathbf{s}_i||_2$, and since $||\boldsymbol{\mu}-\mathbf{s}_i||_2$ is the distance between the previous observation ($\mathbf{s}_i$) and the spatial attractor ($\boldsymbol{\mu}$), $\tau \in (0,1)$ indicates the fraction of that distance that is covered by $\vec{\mathbf{F}}_i$. Parameter τ can then be interpreted as the strength of attraction, since the larger it is, the larger is ξ_i. In detail, we obtain $\lim_{\tau\to 1}\mathbb{E}(\mathbf{s}_{i+1}|\mathbf{s}_i)=\boldsymbol{\mu}$ and $\lim_{\tau\to 1}\xi_i=||\boldsymbol{\mu}-\mathbf{s}_i||_2$, which indicates that if $\tau\to 1$ the mean of the conditional distribution of $\mathbf{s}_{i+1}$ is on the coordinate $\boldsymbol{\mu}$ and the position at time $i+1$ is then centered on the attractor. On the other hand, if $\tau\to 0$, there is no attraction since $\lim_{\tau\to 0}\mathbb{E}(\mathbf{s}_{i+1}|\mathbf{s}_i)=\mathbf{s}_i$ and $\lim_{\tau\to 0}\xi_i=0$, and the model reduces to a random walk. Unlike the CRW, the variability of the movement in the fixed reference frame is constant, as can be seen from the covariance matrices of $\mathbf{v}_i$ and $\mathbf{s}_i$.

Some examples of the BRW can be seen in Figure 3 (b), where the described characteristics are easy to identify. Each vector $\vec{\mathbf{F}}_i$ (solid arrow) points to the spatial attractor $\boldsymbol{\mu}=(0,0)'$ (black dot), its direction is independent of the previous movement direction (the dashed arrow) and depends only on the relative position with respect to the attractor. Since $\tau=0.25$, the length of any $\vec{\mathbf{F}}_i$ is equal to 25% of the distance between $\mathbf{s}_i$ (the tail of $\vec{\mathbf{F}}_i$) and the spatial attractor (the dot). All the ellipses have the same shape, and are only translated in space, which means that the covariance matrix does not depend on the location $\mathbf{s}_i$ or on the previous bearing-angle ϕ_{i-1}.

2.4. *Step and turn with an attractive point.* In this section, we introduce the main contribution of this work, that is a way to model a path that has the CRW and BRW of the previous two sections as special cases, and which can exhibit, with different degrees, directional persistence and an attraction to a point in space. Our idea is to introduce a parameter $\rho\in[0,1]$, and to define $\vec{\mathbf{F}}_i$ as a weighted mean between the vector $\vec{\mathbf{F}}_i$ in the CRW and the BRW, with weights equal to ρ and $1-\rho$, respectively. We then obtain, in terms of equation (1), $\mathbf{M}_i=(1-\rho)\tau\,(\boldsymbol{\mu}-\mathbf{s}_i)+\rho\mathbf{R}(\phi_{i-1})\boldsymbol{\eta}$, where it is clear that the values of ρ that are close to 0 indicate a strong central place attraction and weak directional persistence, while values of ρ that are close to 1 indicate a weak central place attraction and a strong directional persistence. The length and direction of $\vec{\mathbf{F}}_i$ change smoothly with ρ.

In order to specify the conditional distribution of $\mathbf{s}_{i+1}$, we need its covariance matrix. As shown in the previous sections, the covariance matrix for the BRW is fixed (equation (14)), while it depends on the previous bearing-angle for the CRW (equation (11)). Our aim is for the covariance to change smoothly from $\boldsymbol{\Sigma}$ to $\mathbf{R}(\phi_{i-1})\boldsymbol{\Sigma}\mathbf{R}'(\phi_{i-1})$, on the basis of the value ρ, and since the rotation matrix reduces to an identity matrix when its argument is zero, and a smaller argument than ϕ_{i-1} rotates the matrix by less than ϕ_{i-1}, we define the variance as $\mathbf{V}_i=\mathbf{R}(\rho\phi_{i-1})\boldsymbol{\Sigma}\mathbf{R}'(\rho\phi_{i-1})$. The conditional distribution of the path therefore becomes

$$\mathbf{s}_{i+1}|\mathbf{s}_i,\mathbf{s}_{i-1}\sim N(\mathbf{s}_i+(1-\rho)\tau\,(\boldsymbol{\mu}-\mathbf{s}_i)+\rho\mathbf{R}(\phi_{i-1})\boldsymbol{\eta},\mathbf{R}(\rho\phi_{i-1})\boldsymbol{\Sigma}\mathbf{R}'(\rho\phi_{i-1})), \tag{17}$$

which is second-order Markovian. If the path follows equation (17), we say that it is a STAP. The parameters in (17) are $\boldsymbol{\mu}$, $\boldsymbol{\eta}$, $\boldsymbol{\Sigma}$, τ, ρ and $\mathbf{s}_0$. Examples based on the CRW and BRW in Figures 3 (a) and (b) are shown in Figures 3 (c) and (d), for two values of ρ. We can see that the STAP is closer to the BRW for $\rho=1/3$, i.e., the path is attracted

to $\boldsymbol{\mu}$ and there is a modest directional persistence, while the STAP resembles a CRW more for $\rho = 2/3$, i.e., there is a strong directional persistence but the movement is only slightly attracted to $\boldsymbol{\mu}$. Using equations (5) and (7), we can find the distribution of the displacement-coordinates

$$\mathbf{v}_i|\mathbf{v}_{i-1},\dots,\mathbf{v}_1 \sim N((1-\rho)\tau\left(\boldsymbol{\mu}-\mathbf{s}_i\right)+\rho\mathbf{R}(\phi_{i-1})\boldsymbol{\eta},\mathbf{R}(\rho\phi_{i-1})\boldsymbol{\Sigma}\mathbf{R}'(\rho\phi_{i-1})),$$

$$\mathbf{y}_i|\mathbf{y}_{i-1},\dots,\mathbf{y}_1 \sim N((1-\rho)\mathbf{R}'(\phi_{i-1})\tau\left(\boldsymbol{\mu}-\mathbf{s}_i\right)+\rho\boldsymbol{\eta},\mathbf{R}(\phi_{i-1}(\rho-1))\boldsymbol{\Sigma}\mathbf{R}'(\phi_{i-1}(\rho-1))),$$

where, for the conditional distribution of $\mathbf{y}_i$ we use the following properties of the rotation matrix: $\mathbf{R}^{-1}(w)=\mathbf{R}'(w)=\mathbf{R}(-w)$ and $\mathbf{R}(w_1)\mathbf{R}(w_2)=\mathbf{R}(w_1+w_2)$. From the above equation, it is clear that the displacement-coordinates are not identically distributed and the movement-metrics are location-dependent.

It should be noted that the STAP can only be defined for observations that are equally-spaced in time. This is due to its CRW component which, as discussed in Section 2.2, presents challenges for the definition of the conditional density for non constant time-intervals.

2.5. *Hidden Markov model.* If we assume that the animal exhibits different behaviors in the observed time-window, the STAP model, as proposed in (17), may not be flexible enough to be used to model the data, since different movement characteristics should be modeled by different parameters, while the parameters in equation (17) do not change over time. For this reason, trajectory tracking data are generally assumed to originate from a mixture-type model in which the latent cluster-membership variable $z_i \in Z \subseteq \mathbb{N}$ is interpreted as a behavior indicator, so that $z_i = j$ means that, at time i, the animal is following j-th behavior. We can easily link the behavior to the STAP parameters by assuming $\mathbf{s}_{i+1}|\mathbf{s}_i,\mathbf{s}_{i-1} \sim N\left(\mathbf{s}_i+\mathbf{M}_{i,z_i},\mathbf{V}_{i,z_i}\right)$ with

$$\mathbf{M}_{i,z_i} = (1-\rho_{z_i})\tau_{z_i}\left(\boldsymbol{\mu}_{z_i}-\mathbf{s}_i\right)+\rho_{z_i}\mathbf{R}(\phi_{i-1})\boldsymbol{\eta}_{z_i}, \tag{18}$$

$$\mathbf{V}_{i,z_i} = \mathbf{R}(\rho_{z_i}\phi_{i-1})\boldsymbol{\Sigma}_{z_i}\mathbf{R}'(\rho_{z_i}\phi_{i-1}). \tag{19}$$

In both (18) and (19), the parameters are indexed by the latent variable z_i and they therefore change according to the animal's behavior at time i. The set $(\rho_j,\tau_j,\boldsymbol{\mu}_j,\boldsymbol{\eta}_j,\boldsymbol{\Sigma}_j)$ contains the STAP parameters that describe the j-th behavior and, for example, if $\rho_1 = 1$, $\rho_2 = 0$ and $\rho_3 = 0.5$, the first behavior is a BRW, the second a CRW and the third is a BCRW.

Different approaches have been proposed to model z_i, and the most commonly used is the HMM where the temporal evolution of z_i is generated by a first-order Markov process, so that $\mathbb{P}(z_i = j|z_{i-1},\dots,z_1) = \mathbb{P}(z_i = j|z_{i-1}) = \pi_{z_{i-1},j}$ for $i \in \{1,\dots,T-1\}$, where the probability depends on the previous behavior and z_0 is here equal to 1. Generally, z_i is assumed to have values in the set $\{1,2,\dots,K^*\}$, where K^* indicates the maximum number of behaviors that we expect to see between time 1 and $T-1$, and the optimal K^* is chosen by considering the opinion of experts or information criteria. Instead of using a model with a finite K^*, we propose modeling the data with the sHDP-HMM of Fox *et al.* (2011), using the STAP as the emission-distribution. In the sHDP-HMM, we have $Z \equiv \mathcal{N}$, i.e., there are infinite possible behaviors but, with a finite number of time-points, only a finite number of them, K, can be observed (these are called "non-empty states" (Frühwirth-Schnatter and Malsiner-Walli, 2019)), and the random variable K is used to estimate the number of behaviors. The HMM component of the model is non-parametric, since the number of possible behaviors is assumed to

be countable and unbounded, and K is a random variable that can be estimated. The proposed HMM model, which we call STAP-HMM, is

$$
\begin{aligned}
\mathbf{s}_{i+1}|\mathbf{s}_i, \mathbf{s}_{i-1}, \mathbf{M}_{i,z_i}, \mathbf{V}_{i,z_i} &\sim N\left(\mathbf{s}_i + \mathbf{M}_{i,z_i}, \mathbf{V}_{i,z_i}\right), \\
z_i|z_{i-1}, \boldsymbol{\pi}_{z_{i-1}} &\sim \text{Multinomial}(1, \boldsymbol{\pi}_{z_{i-1}}), \\
\boldsymbol{\pi}_j|\alpha, \kappa, \boldsymbol{\beta} &\sim \text{Dir}\left(\alpha + \kappa, \frac{\alpha\boldsymbol{\beta} + \kappa\delta_j}{\alpha + \kappa}\right), \\
\boldsymbol{\beta}|\gamma &\sim \text{GEM}\left(\gamma\right), \\
\rho_j, \tau_j, \boldsymbol{\mu}_j, \boldsymbol{\eta}_j, \boldsymbol{\Sigma}_j &\sim H,
\end{aligned}
\tag{20}
$$

where $\boldsymbol{\pi}_j$ and $\boldsymbol{\beta}$ are infinite-dimensional probability vectors, GEM$(\cdot)$ indicates the Griffiths-Engen-McCloskey distribution (Ishwaran and Zarepour, 2002), δ_j is the Dirac-delta, and H is a distribution over the likelihood parameters which acts as a prior. We assume a uniform distribution over the observed domain $\mathcal{D}$ for parameter $\mathbf{s}_0$.

For distribution H, we assume independence between the parameters with a normal distribution for $\boldsymbol{\mu}_j$ and $\boldsymbol{\eta}_j$, an inverse-Wishart for $\boldsymbol{\Sigma}_j$, and a uniform distribution over $(0,1)$ for ϕ_j. We want to be able to tell whether a behavior is a CRW ($\rho_j = 1$), a BRW ($\rho_j = 0$) or a BCRW ($\rho_j \in (0,1)$), which means that we must allow ρ_j to assume, a posteriori, not only values in $(0,1)$, but also 0 or 1. This can be done by assuming a mixed-type distribution over ρ_j, which then becomes a mixed-type random variable composed of a discrete distribution with probabilities $w_0 > 0$ and $w_1 > 0$ on 0 and 1, respectively, and a distribution over $(0,1)$, which, in our case, is the uniform distribution, with an associated weight $w_{(0,1)} > 0$; in order to obtain a proper distribution, it is necessary to have $w_0 + w_1 + w_{(0,1)} = 1$. The cumulative distribution function of the distribution over ρ_j is

$$
\mathbb{P}(\rho_j \leq d) = \begin{cases} 0 & \text{if } d < 0, \\ w_0 & \text{if } d = 0, \\ w_0 + w_{(0,1)} d & \text{if } 0 < d < 1, \\ w_0 + w_{(0,1)} + w_1 = 1 & \text{if } d \geq 1. \end{cases}
\tag{21}
$$

We consider the use of a mixed-type distribution over ρ_j as being an important contribution of this work, since it allows us to easily detect the type of behavior. We also assume (α, κ, γ) to be random variables and, following Fox *et al.* (2011), closed-form expressions for the updating of these parameters can be achieved with the following priors: $\alpha + \kappa \sim G(a_1, b_1)$, $\kappa/(\alpha + \kappa) \sim B\left(a_2, b_2\right)$, and $\gamma \sim G(a_3, b_3)$, where $B(\cdot,\cdot)$ stands for the Beta distribution and $G(\cdot,\cdot)$ for the Gamma. Missing observations are also considered as parameters that have to be estimated. Since we are directly modeling the path, the posterior distribution of the missing data is coherent with the observed locations, and we do not need any further assumptions, as instead are needed in Jonsen *et al.* (2005) and McClintock *et al.* (2012), where the missing locations are assumed to be on the line connecting the previous and subsequent observed locations.

The suggested distributions allow the implementation of MCMC updates based on Gibbs steps, with the only exceptions being ρ_j and the missing data, as shown in Appendix A.

2.6. *Differences in and similarities between the STAP-HMM and the McClintock et al. (2012) proposal.* The McClintock *et al.* (2012) model is a general framework for BCRWs that generalizes most of the other approaches. It shares some similarities with

our proposal and can be considered its main competitor, since it is an HMM with an emission distribution that has directional persistence and attractive points as it most prominent features. Instead of coordinates, it models the step-length and bearing-angle assuming independence between the two components; the same model can be expressed using the turning-angle instead of the bearing-angle (see equation (9)). Even though independence between the step-length and bearing-angle is not strictly necessary, and their framework can still be used without it, there are very few distributions over the cylinder that can accommodate dependence between circular and linear variables, see, for example, Abe and Ley (2017), Mastrantonio (2018) and references therein. The main idea of McClintock *et al.* (2012) is to define the circular mean $\lambda_{i,j}^{\text{mc}}$ of the angular variable, in the j-th behavior, as a weighted average between the previous direction and the direction of the spatial attractor: $\lambda_{i,j}^{\text{mc}} = \rho_j^{\text{mc}}\phi_{i-1} + (1-\rho_j^{\text{mc}})\zeta_i$, where ζ_i is the angle of the vector connecting $\mathbf{s}_i$ and the attractor, and ρ_j^{mc} is the weight of the j-th behavior. Indeed, as in our proposal, with $\rho_j^{\text{mc}} = 1$ the model reduces to a CRW and $\rho_j^{\text{mc}} = 0$ defines a BRW, while a behavior with $\rho_j^{\text{mc}} \in (0,1)$ has both characteristics. Other parameters of the movement-metrics are modeled to take into account that other movement characteristics, such as circular variance and mean velocity, can be affected by the distance from the attractor. A more detailed description of one of the possible formulations of the model can be found in Appendix C.

Although the McClintock *et al.* (2012) approach is similar to our proposal and it introduces the same features, there are some differences. The McClintock *et al.* (2012) approach is defined using unimodal and symmetric circular distributions, and such distributions are necessary to be able to interpret the results. To understand why, let us suppose that the movement is ruled by a bimodal circular distribution, which is a mixture of two wrapped-Cauchy with means $\lambda_{i,j}^{\text{mc}} + \pi/3$ and $\lambda_{i,j}^{\text{mc}} - \pi/3$, small circular variances, and equal weights. In this case, the circular mean is $\lambda_{i,j}^{\text{mc}}$ and, if $\rho_j^{\text{mc}} = 0$, the model reduces to a BRW, and $\lambda_{i,j}^{\text{mc}} = \zeta_i$ is therefore the direction of the attractor. Since there are two modes and the circular variance of the two components is small, even though the model is a BRW, the density of the circular distribution over the direction ζ_i is almost zero, which means that the animal never goes toward the attractor, but is more likely to be in a direction close to $\zeta_i + \pi/3$ or $\zeta_i - \pi/3$. We then lose the possibility of modeling and interpreting the attractor in a meaningful way. A similar issue can arise if the circular mean is modeled with a non symmetrical distribution. On the other hand, the circular distribution of our proposal is highly flexible, as shown in Figure 2, and we do not have the same problem as McClintock *et al.* (2012), since we are modeling the coordinates, and the mean of the conditional normal density of $\mathbf{s}_{i+1}$ depends on the location of the attractor. In our proposal, the characteristics of the distribution of the movement-metrics (e.g., means and variances) change according to the distance from the attractor and the previous bearing-angle (see Section 2.4), but there is no need to model them directly.

We also want to show that a bimodal circular distribution can be helpful to describe an animal's path, especially in a CRW. Even if, for a given time-interval, for example 10 minutes, the turning-angle of a CRW is distributed as a unimodal and symmetric distribution, e.g., a wrapped-Cauchy, if we record the data with a different time-interval, e.g., 20 minutes, and we use the recorded data to compute the turning-angle, this may be distributed as a multimodal or asymmetric distribution, as is possible to see in the simulated data in Appendix D. To further clarify this point, we here show a simple example. Let us suppose that the true path of an animal for a time-interval of 10 minutes is described by a wrapped-Cauchy with a circular mean π (half a circle), the step-length is Weibull distributed with a mean of 1, and both distributions have a small

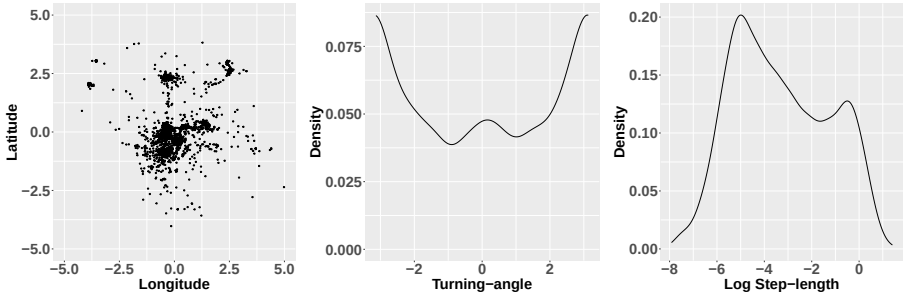

(a) (b)

Fig 4: Observed coordinates (a) and kernel density estimates of movement-metric distributions ((b) and (c)).

variance. If $\mathbf{s}_1 = (0,0)'$, and $\phi_0 = 0$, we can expect $\mathbf{s}_2$ to be close to the spatial point $(-1,0)'$, $\mathbf{s}_3$ to be close to $(0,0)'$, and, since the variances of the distributions are small, we expect $s_{3,2} \approx 0$. This means that $\mathbb{P}(s_{3,1} < 0) \approx 0.5$, i.e., half of the time the step-length of time $i = 1$ is larger than the step-length of time $i = 2$, and $\mathbb{P}(s_{3,1} \geq 0) \approx 0.5$, i.e., half of the time the opposite is true. If we record the data with a time-interval of 20 minutes, the first turning-angle is computed as

$$\theta_1 = \text{atan}^*(s_{3,2} - s_{1,2}, s_{3,1} - s_{1,1}) - \phi_0 = \text{atan}^*(s_{3,2} - s_{1,2}, s_{3,1} - s_{1,1}),$$

see equation (8), because the second recorded coordinate is $\mathbf{s}_3$. Then, since $s_{3,2} \approx 0$, $\mathbb{P}(s_{3,1} < 0) \approx 0.5$ and $\mathbb{P}(s_{3,1} \geq 0) \approx 0.5$, we obtain $\mathbb{P}(\theta_1 \in \partial 0) \approx 0.5$ and $\mathbb{P}(\theta_1 \in \partial \pi) \approx 0.5$, where $\partial 0$ and $\partial \pi$ denote small sections around 0 and π, respectively. This means that the circular distribution is unimodal for a time-interval of 10 minutes, while, if we record the data with a time-interval of 20 minutes, it is bimodal with two modes at ≈ 0 and $\approx \pi$. When data are available, we cannot know if the turning-angle distribution recorded at the given time-interval is unimodal and symmetric and we should therefore use a distribution that can also take into account asymmetry and multimodality, which is not possible with the model of McClintock *et al.* (2012), but is, instead, a by-product of our proposal, see Figure 2.

The McClintock *et al.* (2012) framework in the original Bayesian model and the new frequentist implementation in the *momentuHMM* *R*-package (McClintock and Michelot, 2018), both require the number of behaviors to be fixed in order to estimate the model, but this is not necessary in the STAP-HMM. Moreover, the prior on ρ_j allows us to detect the behavior-type, while the McClintock *et al.* (2012) approach requires an RJMCMC to obtain the same result, or the use of informational criteria, such as the AIC in the *momentuHMM* *R*-package. The RJMCMC is an algorithm which, apart from other problems, presents challenges in its implementation and in the designing of a valid trans-dimensional proposal (Hastie and Green, 2012), especially since it is not possible to find a closed-form full conditional for most likelihood parameters, and Metropolis steps need to be used. On the other hand, our MCMC is mostly based on Gibbs steps, and it does not need a trans-dimensional MCMC. Moreover, working directly with coordinates instead of movement-metrics allows us to easily estimate any missing locations as part of the model fitting, and without imposing any constraints, apart from the missing observations to only have a positive density in $\mathcal{D}$, while McClintock *et al.* (2012) assumes linearity between non-missing points.

3. Real data. Maremma Sheepdogs are large-breed dogs, originating from Italy, that have been used for centuries all over Europe and Asia to protect livestock from predators and thieves. These dog are trained, from an early age, to live with livestock, thereby creating a strong bond, and adult dogs therefore view the livestock as their social companions and protect them from threats for the rest of their lives. Recent studies have proved that Sheepdogs are effective in protecting livestock from a wide range of potential predators (Gehring *et al.*, 2017; van Bommel and Johnson, 2016). The dogs can be fence-trained, to remain in the proximity of the paddock where the livestock are confined, but they are generally allowed to cross fences, move freely and roam over large areas. The use of Maremma Sheepdogs (or general livestock guardian dogs) is relatively new in Australia and outside the country of origin, and interest in their use is increasing (van Bommel and Invasive Animals Cooperative Research Centre, 2010). Owing to the extension of the properties, which can be several thousand squared hectares, it is hard, or even impossible, for an owner to supervise dogs (van Bommel and Johnson, 2012), which are visited rarely, and sometimes only once a week.

The dataset[1] contains GPS locations of Maremma Sheepdogs and sheep on three properties (van and Johnson, 2014). From the available data, we selected a subset of temporally-contiguous observations of one female dog, called "Bindi", who belongs to the "Rivesdale" property, situated in North-East Victoria. Bindi's locations were recorded every 30 minutes, starting from 2010-03-13 at 18:30, to 2010-07-23 at 17:33. The data, which consist of 6335 time-points with 196 missing observations, are plotted in Figure 4 (a); it should be noted that, to facilitate the specification of the priors, the coordinates are centered and divided by a pooled variance. The kernel density estimates of the observed movement-metrics are depicted in Figures 4 (b) and (c), where we can see bimodality in both the log step-length and turning-angle, thus suggesting a CRW, while attractive points are suggested from Figure 4 (a), e.g., around coordinates (0,0), which could lead to a BRW.

Owing to the still recent use of these dogs in Australia, and given the extension of the property, the owner is often unaware of the dog's movements and how she behaves (van Bommel and Invasive Animals Cooperative Research Centre, 2010). In this work, we are interested in finding how many behaviors the dog has and to describe them. We are interested in evaluating the behavior when she is looking after the livestock, at the core of the home-range, and at what time of the day she is more likely to leave the sheep unattended. The description of the movement outside the central core area is also interesting, because it can be related to the dog protecting livestock from predators and be considered evidence of the effectiveness of such dogs.

To the best of our knowledge, this is the first attempt that has been made to identify the number and characteristics of the behavior of a Sheepdog, using a modeling approach. Other works have only described the behavior of a Maremma qualitatively, or have used descriptive statistics (van Bommel and Invasive Animals Cooperative Research Centre, 2010) and tests (van Bommel and Johnson, 2012).

3.1. *Model comparison.* Our aim here is to show that our proposal outperforms the model of McClintock *et al.* (2012) when estimated on the motivating dataset; the performance is evaluated using the DIC_5 of Celeux *et al.* (2006) and the ICL of Biernacki *et al.* (2000), which can easily be computed if no measurement error is assumed.

We use the code provided in the supplementary material of McClintock *et al.* (2012) to estimate their model, modifying it to remove the measurement error. The code

[1] available on https://www.datarepository.movebank.org/handle/10255/move.395

	STAP-HMM	MC-HMM$_{4,5}$	MC-HMM$_{7,2}$	MC-HMM$_{5,4}$	MC-HMM$_{3,6}$	MC-HMM$_{6,2}$
DIC$_5$	**-17290.37**	-16634.912	-16557.948	-16317.222	-16012.851	-15727.025
ICL	**13245.672**	9082.2480	8818.4409	8673.5212	8773.3074	8421.2723

TABLE 1

The table shows the DIC$_5$ and the ICL for the STAP-HMM and the 5 best MC-HMM$_{n_b^{mc},n_c^{mc}}$. The model selected by each index is indicated in bold.

estimates an HMM with a given number of BCRW and CRW (which McClintock *et al.* (2012) called "exploratory state") and we indicate as MC-HMM$_{n_b^{\text{mc}},n_c^{\text{mc}}}$ the model of McClintock *et al.* (2012) which is based on n_b^{mc} BCRW and n_c^{mc} CRW behaviors. An RJMCMC is exploited to choose between different parametrizations that allow a BCRW to be reduced to a BRW, thus making it possibility to determine the behavior-type. The emission distribution is the product of a Weibull distribution on the step-length and of a wrapped-Cauchy for the bearing-angle; these distributions are commonly used, see, for example, Morales *et al.* (2004) and Michelot *et al.* (2016). The directional persistence and attraction to the central location is introduced by modeling the wrapped-Cauchy circular mean, and the distance from the center-of-attraction is also used to model the circular concentration and the two Weibull parameters. We use the priors suggested in the original paper, which are shown in Appendix C together with more details on the model formalization.

For our proposal, we use weakly informative priors for the likelihood parameters, namely $N(\mathbf{0}_2, 1000\mathbf{I}_2)$ for $\boldsymbol{\mu}_j$ and $\boldsymbol{\eta}_j$, $\boldsymbol{\Sigma}_j \sim IW(3, \mathbf{I}_2)$, a uniform over $(0,1)$ for ϕ_j. The three weights w_0, w_1, and $w_{(0,1)}$, which define the prior of ρ_j, (see equation (21)) are all equal to $1/3$. We also assume the priors $\alpha + \kappa \sim G(0.1, 1)$, $\kappa/(\alpha + \kappa) \sim B(10, 1)$, $\gamma \sim G(0.1, 1)$, which are defined to avoid the production of redundant behaviors, i.e., behaviors with similar vectors of the likelihood parameters (see Fox *et al.* (2011)), since they induce a distribution over K which is almost fully concentrated on 1. The distribution over K has been evaluated by simulating datasets from the STAP-HMM with the same number of temporal points as the data we are modeling. This means that we are a priori assuming that only one behavior is observed, i.e., the model is not a mixture, and if the data support the hypothesis of different behaviors, the posterior of K will move away from the prior. The spatial domain where the path is recorded is defined as the square $[-5, 5]^2 \equiv \mathcal{D}$. The STAP-HMM is estimated using an MCMC algorithm, implemented in Julia 1.3 (Bezanson *et al.*, 2017). All the models have 5000 posterior samples, based on 125000 iterations, burnin 75000, thin 10. The codes that can be used to replicate the results of our proposal are available at `https://github.com/GianlucaMastrantonio/STAP_HMM_model`.

We decided to test MC-HMM$_{n_b^{\text{mc}},n_c^{\text{mc}}}$ with a number of latent behaviors between 2 and 9 and all possible combinations of BCRW and CRW, e.g., with 4 behaviors we tested the following: MC-HMM$_{0,4}$, MC-HMM$_{1,3}$, MC-HMM$_{2,2}$, MC-HMM$_{3,1}$, and MC-HMM$_{4,0}$. We selected 9 as the maximum number of behaviors since it is reasonable to assume that 10 or more behaviors are not likely to be observed. In fact, such a large number is somewhat uncommon, and the models in literature are usually tested on a maximum of 2 to 5 behaviors (see, for example, Langrock *et al.*, 2012; Pohle *et al.*, 2017; Michelot and Blackwell, 2019). Moreover, we experienced convergence issues and extremely long computation times for models with more than 9 behaviors.

Both DIC$_5$ and ICL are likelihood-based indices and the likelihood of the two approaches must be evaluated on the same data for a fair comparison. For this reason, instead of locations $\mathbf{s}_{i+1}$ we evaluated the likelihood of the STAP-HMM using (r_{i+1}, ψ_{i+1}), whose density can easily be determined from the displacement-coordinates distribution

using standard results (see, for example, Mastrantonio, 2018). We show the computed DIC_5 and ICL for the STAP-HMM and the best five MC-HMM$_{n^b,n^c}$ in Table 1, which are the same for both indices. ICL and DIC_5 select our proposal as the best model and 4 out of 5 MC-HMM$_{n^b,n^c}$ have 9 behaviors, while the other has 8. In order to compute the estimated number of behaviors with the STAP-HMM, we can use the posterior samples. Let K^b be the number of unique values of $\{z_i\}_{i=1}^{T-1}$ in the b-th MCMC iteration, K^b is therefore a posterior sample of K and the set $\{K^b\}_1^{5000}$ can be used to estimate the distribution of the number of observed behaviors (K); we found that $\mathbb{P}(K=5|\mathbf{s}) \approx 0.996$ and $\mathbb{P}(K=6|\mathbf{s}) \approx 0.004$. These results and the ones in Appendix E, where we show that the number of behaviors with the highest posterior probability does not change for a wide range of STAP-HMM hyperparameters priors, indicate that only 5 behaviors are needed to describe the data.

The STAP-HMM is not only preferable from the information criteria point of view, but it is also more parsimonious in terms of number of estimated behaviors. Pohle *et al.* (2017) showed, in a large simulation study, that if the emission distribution is not flexible enough, information criteria can select a number of behaviors that is much greater than the real one. Since, as discussed in Section 2.6, the circular distributions used in the general framework of McClintock *et al.* (2012) are not flexible, i.e., they are unimodal and symmetric, and independence is assumed between the step-length and bearing-angle (or turning-angle), we believe that this is why a large number of behaviors are selected. On the other hand, the distributions induced on the movement-metrics by our proposal, especially in terms of turning- and bearing-angle, are quite flexible.

3.2. *The results.* Since the posterior mode of K is almost fully concentrated on 5, we only describe the results obtained with the set of samples that has $K^b = 5$ and, in order to simplify the discussion, we indicate the j-th latent behavior with LB_j. We show the posterior means (indicated using the hat notation $\hat{\cdot}$) and the 95% credible intervals (CIs) for all the model parameters in Table 2. We compute the maximum-at-posteriori estimate of z_i for each time-point, which we indicate with $\hat{z}_i$ and we call it the MAP behavior at time i. We can then associate a MAP behavior to each spatial location and use it to see wheter there are any differences in the spaces utilized by the animal; this information is indicated with dots in Figure 5. The vectors $\vec{\mathbf{F}}_i$ and the predictive conditional distributions of $\mathbf{s}_{i+1}$ are also shown in the same figure. It should be noted that, since the ellipses in Figure 5 are too small for the first two behaviors, we plot the same objects on a smaller spatial scale in Figure 6. The MAP behavior is also used in Figure 7 where, for a given time of the day (half an hour apart), we show the proportion of occurrence of the values of the MAP behaviors.

We can see from $\hat{\rho}_j$ in Table 2, that the first two behaviors are CRW, and the last two are BRW, with a strength of attraction that is moderate in the fourth ($\hat{\tau}_4 = 0.628$) and very strong in the fifth ($\hat{\tau}_5 = 0.985$). The third behavior is close to a random walk since $\hat{\tau}_3 = 0.027$, with a slight direction persistence ($\hat{\rho}_3 = 0.018$). The same information can be deduced from Figures 5 and 6, which also give more insight into the movement characteristics. The predictive distribution of the turning-angle and log step-length are depicted in Figure 8, albeit only for the behaviors that have a strong CRW component (LB_1 and LB_2) since, as discussed in Sections 2.3 and 2.4, the distribution of the movement metrics in BRWs and BCRWs are location-dependent.

The strong attraction present in LB_5 can be seen in Figure 5, since the heads of the vectors $\vec{\mathbf{F}}_i$ are all on the same coordinates, regardless of the spatial location. It is also possible to see the moderate attraction of LB_4 in the same figure. We can see from the CIs of $\boldsymbol{\mu}_4$ and $\boldsymbol{\mu}_5$ that the two attractors are well defined in space and different from

	j=1	j=2	j=3	j=4	j=5
$\hat{\mu}_{j,1}$	-1.26	-0.4	8.317	-0.35	0.179
(CI)	(-63.744 60.201)	(-63.476 60.828)	(-2.394 46.037)	(-0.413 -0.286)	(0.169 0.189)
$\hat{\mu}_{j,2}$	0.579	0.064	4.209	-0.328	-0.404
(CI)	(-60.586 61.246)	(-62.861 62.019)	(-6.944 32.779)	(-0.4 -0.261)	(-0.413 -0.395)
$\hat{\eta}_{j,1}$	-0.005	-0.045	23.83	-0.068	-0.037
(CI)	(-0.006 -0.004)	(-0.06 -0.03)	(3.257 64.705)	(-60.042 61.38)	(-62.237 61.557)
$\hat{\eta}_{j,2}$	0	-0.001	-5.239	-0.261	0.275
(CI)	(-0.001 0.001)	(-0.012 0.01)	(-21.373 2.178)	(-60.86 62.259)	(-61.478 62.021)
$\hat{\tau}_j$	0.499	0.492	0.027	0.628	0.985
(CI)	(0.024 0.97)	(0.026 0.973)	(0.001 0.079)	(0.574 0.685)	(0.973 0.997)
$\hat{\rho}_j$	1	1	0.018	0	0
(CI)	[1 1]	(1 1]	(0.003 0.071)	[0 0)	[0 0]
$\hat{\mathbf{\Sigma}}_{j,1,1}$	0.001	0.029	0.791	0.128	0.006
(CI)	(0.001 0.001)	(0.022 0.039)	(0.67 0.953)	(0.104 0.158)	(0.005 0.008)
$\hat{\mathbf{\Sigma}}_{j,1,2}$	0	0	-0.078	0.033	0.001
(CI)	(0 0)	(-0.002 0.002)	(-0.139 -0.024)	(0.018 0.049)	(0 0.001)
$\hat{\mathbf{\Sigma}}_{j,2,2}$	0.001	0.018	0.373	0.168	0.005
(CI)	(0.001 0.001)	(0.014 0.023)	(0.315 0.444)	(0.14 0.201)	(0.004 0.006)
$\hat{\pi}_{1,j}$	0.848	0.073	0.023	0.044	0.011
(CI)	(0.835 0.861)	(0.063 0.084)	(0.016 0.031)	(0.035 0.055)	(0.005 0.019)
$\hat{\pi}_{2,j}$	0.286	0.388	0.145	0.094	0.086
(CI)	(0.242 0.336)	(0.335 0.44)	(0.109 0.185)	(0.057 0.135)	(0.057 0.116)
$\hat{\pi}_{3,j}$	0.066	0.202	0.513	0.162	0.056
(CI)	(0.037 0.102)	(0.143 0.268)	(0.441 0.581)	(0.114 0.218)	(0.027 0.092)
$\hat{\pi}_{4,j}$	0.169	0.206	0.001	0.419	0.205
(CI)	(0.125 0.218)	(0.145 0.272)	(0 0.018)	(0.343 0.493)	(0.161 0.252)
$\hat{\pi}_{5,j}$	0.873	0	0.008	0.003	0.116
(CI)	(0.768 0.976)	(0 0.003)	(0 0.035)	(0 0.027)	(0.018 0.217)
$\hat{\beta}_j$	0.248	0.169	0.14	0.172	0.219
(CI)	(0.079 0.484)	(0.039 0.373)	(0.023 0.341)	(0.039 0.375)	(0.065 0.439)

	α	κ	γ
$\hat{}$	0.284	2.701	1.177
(CI)	(0.007 1.073)	(1.408 4.447)	(0.296 2.754)

TABLE 2

Posterior means and 95% CIs of the STAP-HMM parameters for K=5.

each other. On the other hand, the length of $\vec{\mathbf{F}}_i$ is approximatively zero in the first two behaviors, see Figure 6, but the variance of the conditional distribution of $\mathbf{s}_{i+1}$ rotates with the bearing-angle (see the direction of the major axis of the ellipses) which is a characteristic of directional persistence. Figure 8 shows that LB_1 has a slower speed than LB_2 and both have a bimodal circular distribution with the major mode at around $-\pi$ and a smaller one at 0. These modes indicate that the dog tends to move in the opposite direction to the previous movement (mode at $-\pi$) or in the same direction (mode at 0). The vector $\vec{\mathbf{F}}_i$ in LB_3 changes slightly according to the spatial location, but the attractor is not well defined in space since the CI of $\boldsymbol{\mu}_3$ is large and contains the entire space where the animal has been observed. It should be noted that the major axis of the ellipses rotate slightly in Figure 5 (c), thus suggesting a very small directional persistence.

In Appendix G, we show simulated coordinates from the STAP-HMM, obtained using the posterior means in Table 2 as parameters, where we can see that the coordinates have the data characteristic, for example the central bulk of observations, as well as the extension of the "explored space". The results that are obtained when we only consider CRW (CRW-HMM) or BRW behaviors (BRW-HMM) are also discussed in Appendix G.

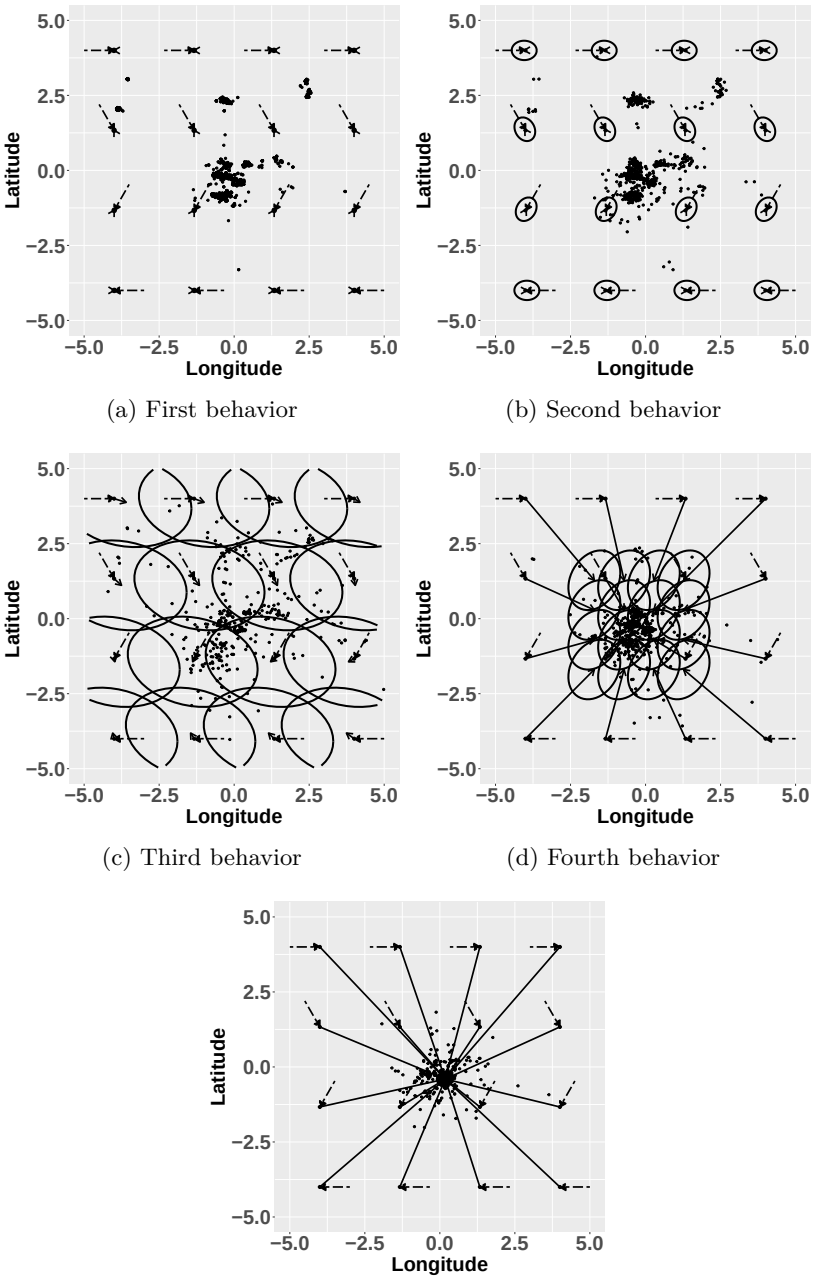

(a) First behavior

(b) Second behavior

(c) Third behavior

(d) Fourth behavior

(e) Fifth behavior

Fig 5: Graphical representation of the predictive conditional distribution of $\mathbf{s}_{i+1}$ for different possible values of $\mathbf{s}_i$ and previous directions. The dashed arrow represents the movement between $\mathbf{s}_{i-1}$ and $\mathbf{s}_i$. The solid arrow is $\vec{\mathbf{F}}_i$, while the ellipse represents an area containing 95% of the probability mass of the predictive conditional distribution of $\mathbf{s}_{i+1}$, computed using (2). The dots for the j-th figure are the coordinates for which $\hat{z}_i = j$.

Behavior description. It is clear from the posterior mean of $\pi_{j,k}$ and from Figure 7 that the animal spends most of her time in LB_1. By comparing the spatial coordinates

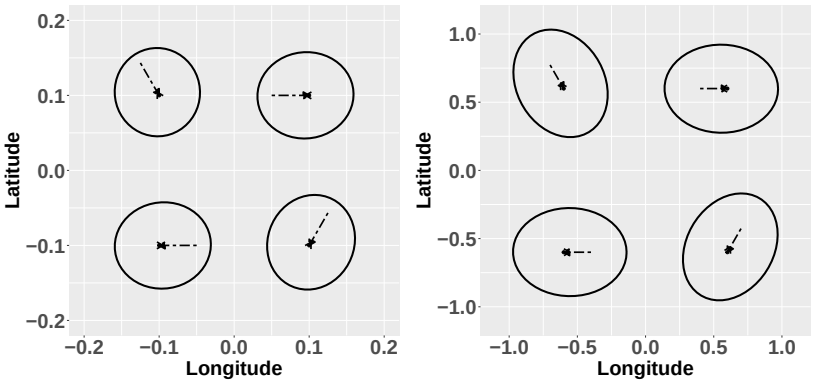

(a) First behavior (b) Second behavior

Fig 6: Graphical representation of the predictive conditional distribution of $\mathbf{s}_{i+1}$ for different possible values of $\mathbf{s}_i$ and previous directions for the first two behaviors at greater spatial detail than in Figure 5. The dashed arrow represents the movement between $\mathbf{s}_{i-1}$ and $\mathbf{s}_i$. The solid arrow is $\vec{\mathbf{F}}_i$, while the ellipse represents an area containing 95% of the probability mass of the predictive conditional distribution of $\mathbf{s}_{i+1}$, computed using (2).

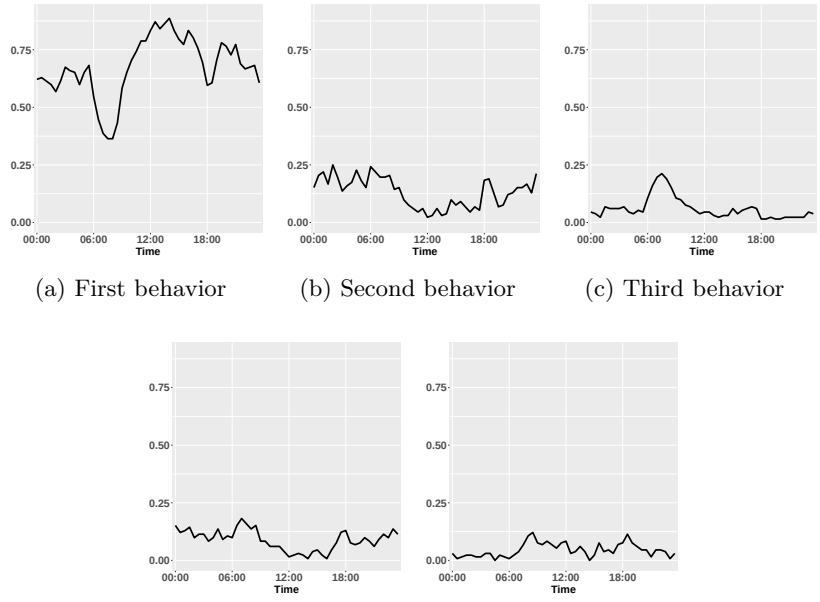

(a) First behavior (b) Second behavior (c) Third behavior

(d) Fourth behavior (e) Fifth behavior

Fig 7: The values of the lines at each time (x-axis) represent the proportion of the times that the STAP-HMM MAP behaviors are observed (y-axis).

of LB_1, shown in Figure 5 (a), with the property boundaries in Figure G.2, we can see that the animal mostly stays inside the property boundaries. This consideration, together with the low speed and the changes in direction (Figure 8), allows us interpret it as boundary-patrolling or scent-marking behavior, which has already been observed

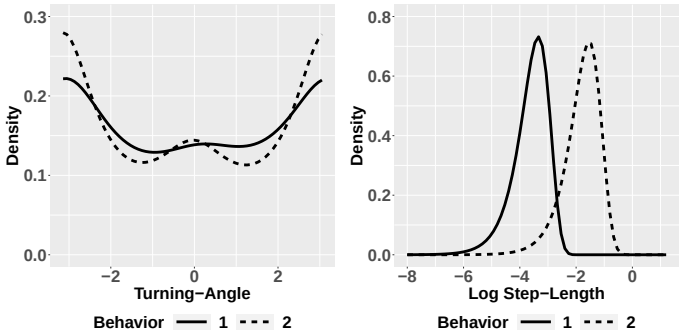

(a) (b)

Fig 8: Turning-angle (a) and log step-length (b) predictive distributions for the first two behaviors of the STAP-HMM. The distributions are computed using only the CRW component.

for other livestock guardian dogs (McGrew and Blakesley, 1982). The probability of observing LB_1 drops in the early morning and late afternoon, and it is smaller during the night than for the central hours of the day.

Regarding LB_2, the higher speed and the smaller variance in the turning-angle distribution with respect to LB_1, the spatial coordinates that are very similar to those of LB_1, and the fact that it is more likely during the night and the afternoon, are all clues that, with this behavior, the animal could be defending the territory from predators, which is coherent with the known behavior of potential predators that are present in the area where the data were collected (Brook *et al.*, 2012; Walton *et al.*, 2017).

There is also an increase in the probability of LB_3 in the first hours of the day, which is otherwise very small. This is the behavior with the largest variability in the observed coordinates (Figure 5 (c)) and an almost total absence of structure in the movement, from both the CRW and BRW points-of-view. With this behavior, the animal is exploring, going outside the property boundaries and also visiting nearby sheep flocks (see van Bommel and Johnson, 2014). If the dog leaves LB_3, the probability of switching to LB_1 and LB_5 is small ($\hat{\pi}_{3,1}/(1-\hat{\pi}_{3,3}) = 0.135$ and $\hat{\pi}_{3,4}/(1-\hat{\pi}_{3,3}) = 0.115$), while the probability of going to LB_4 ($\hat{\pi}_{3,4}/(1-\hat{\pi}_{3,3}) = 0.333$) and LB_2 ($\hat{\pi}_{3,2}/(1-\hat{\pi}_{3,3}) = 0.415$) is higher; the high probability of LB_2 is likely due to the possibility of spotting a potential predator during the exploration.

LB_4 is one of the behaviors with a well defined attractor, and its spatial coordinates are located in the central area where the sheep are (for completeness, the observed coordinates of the sheep are depicted in the Appendix, Figure G.1). The spatial attractor has a posterior mean $\hat{\boldsymbol{\mu}}_4 = (-0.35, -0.328)'$, which is located in the center of the livestock paddock (for details, see van Bommel and Johnson, 2014). When the dog is close to its attractor, the 95% probability area, represented by the ellipses in Figure 5 (d), is large enough to encompass most of the sheep locations, which means that the dog is moving between the sheep. This is more probable during the night, and two probability spikes can be observed in the early morning and late afternoon when there is a drop in the LB_1 probability. It should be noted that all the previously described behaviors have some coordinates that overlap those of the sheep, but not all of them do, which means that the dog is moving through the space according to a CRW (LB_1 and LB_2) or an RW (LB_3) and the path sometimes overlaps the sheep locations, probably as a way of continuously guarding the livestock while engaging in other activities. On the other hand, when the dog shows this behavior (LB_4), she is attracted to the sheep paddock,

and is more likely to show this behavior during the night, when the sheep are more vulnerable to attacks. This can easily be interpreted as the dog attending the livestock, and the high probability of moving to this behavior from LB_3 ($\hat{\pi}_{3,4}/(1-\hat{\pi}_{3,3}) = 0.333$), i.e., the exploring one, can be interpreted as a way of checking on the livestock after leaving the sheep unsupervised.

In the final behavior, there is a well located attractor and the variability of the movement is very low (the size of the ellipses in Figure 5 (e)), which means that, for any point in space, the animal moves precisely on the coordinate of the attractor. The probability of continuing this behavior is very low ($\hat{\pi}_{5,5} = 0.116$) and the only switching probability with a high value is $\hat{\pi}_{5,1} = 0.873$. In order to interpret this behavior, we can look at Figure G.2, which shows that there is a self-feeder, located approximatively at the spatial location $\hat{\boldsymbol{\mu}}_5$, where the dog can obtain dry food ad-lib. As a result of these considerations, we believe that this can be interpreted as a feeding behavior and, after feeding, the dog switches, with a high probability, to boundary-patrolling.

4. Final remarks. In this work, we have proposed an HMM that is based on a new emission distribution, which we have called STAP, that can be used to model animal movements with attractive points and directional persistence. The STAP belongs to the BCRW family. We have described the similarities to and differences from the model proposed by McClintock *et al.* (2012), which is a generalization of previous approaches that are aimed at combining attraction and directional persistence. Our proposal is easy to implement, is very flexibile, especially in terms of the angular variable distribution, and is easily interpretable. We also introduce a distribution over the likelihood parameters that has allowed us to detect the type of behavior of the dog.

The proposal was estimated on the motivating example, where the spatial locations of a Maremma Sheepdog were recorded. To the best of our knowledge, this work is the first to have used a mixture-model to identify the characteristics of the behavior of a Maremma, and the results we have obtained are clear and easy to interpret. The model is able to find 5 different behaviors, two CRW (LB_1 and LB_2), two BRW (LB_4 and LB_5) and an RW, with slightly directional persistence (LB_3), which is therefore a BCRW. These behaviors are easily characterizable, and they appear to be very different. We found that the dog is on boundary-patrolling for most of the time (LB_1), and when she changes behavior, because she is defending the property (LB_2), exploring the space (LB_3), staying within the sheep paddock (LB_4) or going to the self-feeder (LB_5), she switches back to boundary-patrolling after a few time-points. The information obtained with our model can be used to better understand how to employ these dogs and it suggests that they may be effective in protecting livestock, since the recorded dog constantly guarded the property and livestock and never left for an extensive period of time.

From the obtained results, we can infer that a mixture-type model with a BCRW emission distribution is needed to model such data. As shown in Appendix E, regardless of the priors chosen for the HMM hyper-parameters, 5 was always the number of behaviors with the highest posterior probability, which points out that a mixture-type model is the right approach. The STAP has the CRW and the BRW as special cases, and they can be estimated if the parameter ρ is equal to 1 or 0, respectively. Since between the five behaviors that were found we have CRWs, BRWs and also a BCRW, a density that is able to model all of the three is necessary.

The two CRW behaviors have bimodal posterior predictive distributions, see Figure 8. Since the STAP with the right set of parameters can have a unimodal and symmetric circular density, bimodality was needed to better fit these behaviors. The informational

criteria in Table 1 show that the STAP-HMM is preferable to the model of McClintock *et al.* (2012), and it requires a smaller number of behaviors to describe the data. Hence, there is evidence that the STAP is superior, in terms of description ability, to the emission distributions proposed in McClintock *et al.* (2012). We have shown, in Appendix D, that it is not possible to assume a unimodal and symmetric turning-angle distribution for all time-intervals, which, we believe, is one of the reasons why the model of McClintock *et al.* (2012) needs a large number of behaviors to describe the data. On the other hand, we have shown that the number of estimated behaviors of our proposal does not change even when changing the priors over the STAP-HMM hyperparameters, see Appendix E, which suggests that the animal exhibited 5 different types of behavior in the observed time-window.

In the future, we will extend our model to incorporate several animals, as in Langrock *et al.* (2014), we will use more flexible temporal dynamics for the latent behavior switching, as in Harris and Blackwell (2013) or Mastrantonio *et al.* (2019), and we will also introduce covariates into the emission distribution.

Acknowledgements. The author would like to thank the Editor-in-Chief, the Associate Editor and the two anonymous reviewers for their comments that have greatly improved the manuscript. This work has partially been developed under the MIUR grant Dipartimenti di Eccellenza 2018 - 2022 (E11G18000350001), conferred to the Dipartimento di Scienze Matematiche - DISMA, Politecnico di Torino.

Appendix A Implementation details. In this section, we describe how to sample the STAP parameters and missing observations in the MCMC algorithm, by showing the full conditional distribution, when it can be derived in closed-form, or the proposal distribution used in the Metropolis step, when the full conditional is not available in closed-form. For the sHDP-HMM parameters, the reader can refer to the original paper of Fox *et al.* (2011), where different sample schemes are explained; we used the *degree L weak limit approximation* (Ishwaran and Zarepour, 2002) with $L = 200$ (algorithm 4).

Let $\mathcal{I}_j$ be the set of indices i, so that $z_i = j$, and let n_j be the number of elements in $\mathcal{I}_j$; $\mathcal{I}_j$ can be empty. Given the conditional specification (20), if $n_j > 0$, the likelihood contribution to the full conditional of a STAP parameter, for the $j-th$ behavior, is proportional to

$$\prod_{i \in \mathcal{I}_j} |\boldsymbol{\Sigma}_j|^{-\frac{1}{2}} \exp\left(-\frac{(\mathbf{s}_{i+1} - \mathbf{s}_i - \mathbf{M}_{i,j})' \mathbf{V}_{i,j}^{-1} (\mathbf{s}_{i+1} - \mathbf{s}_i - \mathbf{M}_{i,j})}{2} \right), \tag{22}$$

where we used the relation $|\boldsymbol{\Sigma}_j| = |\mathbf{R}(\rho_j \phi_{i-1}) \boldsymbol{\Sigma}_j \mathbf{R}'(\rho_j \phi_{i-1})|$. It should be noted that if $n_j = 0$, the full conditional of a parameter is equal to its prior.

Parameter $\boldsymbol{\mu}_j$. Since we assume $\boldsymbol{\mu}_j \sim N(\mathbf{B}_{\boldsymbol{\mu}}, \mathbf{W}_{\boldsymbol{\mu}})$, and $\boldsymbol{\mu}_j$ enters linearly into the mean of the conditional distribution of $\mathbf{s}_{i+1}$, standard results (Gelman *et al.*, 1995) show that the full conditional is $\boldsymbol{\mu}_j \sim N(\mathbf{B}_{\boldsymbol{\mu},j}, \mathbf{W}_{\boldsymbol{\mu},j})$ with

$$\mathbf{W}_{\boldsymbol{\mu},j} = \left((1-\rho_j)^2 \tau_j^2 \sum_{i \in \mathcal{I}_j} \mathbf{V}_{i,j}^{-1} + \mathbf{W}_{\boldsymbol{\mu}}^{-1} \right)^{-1},$$

$$\mathbf{B}_{\boldsymbol{\mu},j} = \mathbf{W}_{\boldsymbol{\mu},j} \left((1-\rho_j)\tau_j \sum_{i \in \mathcal{I}_j} \mathbf{V}_{i,j}^{-1} \left(\mathbf{s}_{i+1} - \mathbf{s}_i + (1-\rho_j)\tau_j \mathbf{s}_i - \rho_j \mathbf{R}(\phi_{i-1}) \boldsymbol{\eta}_j \right) + \mathbf{W}_{\boldsymbol{\mu}}^{-1} \mathbf{B}_{\boldsymbol{\mu}} \right).$$

Parameter $\boldsymbol{\eta}_j$. If $\boldsymbol{\eta}_j \sim N(\mathbf{B}_{\boldsymbol{\eta}}, \mathbf{W}_{\boldsymbol{\eta}})$, then, for the same reason as above, the full conditional of $\boldsymbol{\eta}_j$ is $N(\mathbf{B}_{\boldsymbol{\eta},j}, \mathbf{W}_{\boldsymbol{\eta},j})$ with

$$\mathbf{W}_{\boldsymbol{\eta},j} = \left(\rho_j^2 \sum_{i \in \mathcal{I}_j} \mathbf{R}'(\phi_{i-1}) \mathbf{V}_{i,j}^{-1} \mathbf{R}(\phi_{i-1}) + \mathbf{W}_{\boldsymbol{\eta}}^{-1} \right)^{-1},$$

$$\mathbf{B}_{\boldsymbol{\eta},j} = \mathbf{W}_{\boldsymbol{\eta},j} \left(\rho_j \sum_{i \in \mathcal{I}_j} \mathbf{R}'(\phi_{i-1}) \mathbf{V}_{i,j}^{-1} \left(\mathbf{s}_{i+1} - \mathbf{s}_i - (1-\rho_j)\tau_j(\boldsymbol{\mu}_j - \mathbf{s}_i) \right) + \mathbf{W}_{\boldsymbol{\eta}}^{-1} \mathbf{B}_{\boldsymbol{\eta}} \right).$$

Parameter τ_j. Similarly to $\boldsymbol{\mu}_j$ and $\boldsymbol{\eta}_j$, τ_j also enters linearly into the mean of the conditional distribution of $\mathbf{s}_{i+1}$. Since its domain is (0,1) and the prior is uniform, the full conditional is therefore a truncated normal $N(\mathbf{B}_{\tau,j}, \mathbf{W}_{\tau,j})\, I(0,1)$ with

$$\mathbf{W}_{\tau,j} = \left((1-\rho_j)^2 \sum_{i \in \mathcal{I}_j} (\boldsymbol{\mu}_j - \mathbf{s}_i)' \mathbf{V}_{i,j}^{-1} (\boldsymbol{\mu}_j - \mathbf{s}_i) \right)^{-1},$$

$$\mathbf{B}_{\tau,j} = \mathbf{W}_{\tau,j} \left((1-\rho_j) \sum_{i \in \mathcal{I}_j} (\boldsymbol{\mu}_j - \mathbf{s}_i)' \mathbf{V}_{i,j}^{-1} \left(\mathbf{s}_{i+1} - \mathbf{s}_i - \rho_j \mathbf{R}(\phi_{i-1}) \boldsymbol{\eta}_j \right) \right).$$

Parameter $\boldsymbol{\Sigma}_j$. We can express equation (22) as

$$\prod_{i \in \mathcal{I}_j} |\boldsymbol{\Sigma}_j|^{-\frac{1}{2}} \exp\left(-\frac{(\mathbf{R}'(\rho_j \phi_{i-1})(\mathbf{s}_{i+1} - \mathbf{M}_{i,j}))' \boldsymbol{\Sigma}_j^{-1} (\mathbf{R}'(\rho_j \phi_{i-1})(\mathbf{s}_{i+1} - \mathbf{M}_{i,j}))}{2} \right)$$

which shows that $\boldsymbol{\Sigma}_j$ is the covariance of normal densities. Given that the prior is $IW(a_{\boldsymbol{\Sigma}}, \mathbf{C}_{\boldsymbol{\Sigma}})$, the full conditional is $IW(a_{\boldsymbol{\Sigma},j}, \mathbf{C}_{\boldsymbol{\Sigma},j})$ (Gelman *et al.*, 1995) with

$$a_{\boldsymbol{\Sigma},j} = n_j + a_{\boldsymbol{\Sigma}},$$

$$\mathbf{C}_{\boldsymbol{\Sigma},j} = \mathbf{C}_{\boldsymbol{\Sigma}} + \sum_{i \in \mathcal{I}_j} (\mathbf{R}'(\rho_j \phi_{i-1})(\mathbf{s}_{i+1} - \mathbf{M}_{i,j}))(\mathbf{R}'(\rho_j \phi_{i-1})(\mathbf{s}_{i+1} - \mathbf{M}_{i,j}))'.$$

Parameter ρ_j. Parameter ρ_j is part of the rotation matrix argument, and as it is therefore not possible to find a closed-form full conditional, it must be sampled using a Metropolis step. Our suggestion is to propose a new value sampling from a mixed-type distribution composed of two bulks of probability in 0 and 1, and a uniform distribution in $(max(0, \rho_j^* - c), min(1, \rho_j^* + c))$ with $c > 0$, where ρ_j^* is the last accepted ρ_j in the MCMC algorithm. The bulks of probability ensure that ρ_j can assume values 0 and 1 a posteriori, while the parameters of the uniform are defined in order to be able to propose a new value that is close to the previously accepted one.

Missing observations and $\mathbf{s}_0$. A closed-form full conditional cannot be found for the missing observations, and a Metropolis should therefore be used. We suggest proposing a new value of the missing $\mathbf{s}_{i+1}$ sampling from its conditional distribution $N(\mathbf{s}_i + \mathbf{M}_{i,z_i}, \mathbf{V}_{i,z_i})$, since it will simplify the Metropolis ratio. The initial value $\mathbf{s}_0$ is sampled using a Metropolis step with a proposal that is a normal distribution with a mean equal to the previously accepted value of $\mathbf{s}_0$.

Appendix B Simulated examples. We here want to show that the parameters of the STAP-HMM can easily be estimated. For this reason, we simulate synthetic data from an HMM with a fixed number of behaviors and STAP emission distribution, and after model fitting we compare the 95% CI of each parameter with the true value; if the

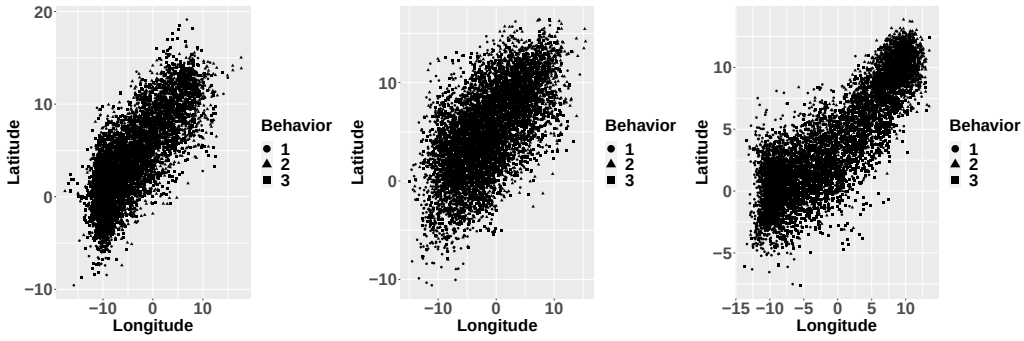

(a) First simulated data (b) Second simulated data (c) Third simulated data

Fig B.1: Locations of the simulated datasets.

latter is inside the CI, we consider the parameter "well estimated". We simulate three datasets with 7000 observations, and 3 behaviors ($K^* = 3$), with $\pi_{j,j} = 0.8$, $\pi_{j,j'} = 0.1$ if $j \neq j'$, and different sets of STAP parameters. In the first dataset, we assume

$$\boldsymbol{\mu}_1 = \begin{pmatrix} -10 \\ 0 \end{pmatrix}, \ \boldsymbol{\mu}_2 = \begin{pmatrix} 10 \\ 10 \end{pmatrix}, \ \boldsymbol{\mu}_3 = \begin{pmatrix} 0 \\ 0 \end{pmatrix}, \ \boldsymbol{\eta}_1 = \begin{pmatrix} 0 \\ 0 \end{pmatrix}, \ \boldsymbol{\eta}_2 = \begin{pmatrix} 1 \\ 1 \end{pmatrix}, \ \boldsymbol{\eta}_3 = \begin{pmatrix} -2 \\ 0 \end{pmatrix},$$

$$\boldsymbol{\Sigma}_1 = \begin{pmatrix} 0.5 & 0.0 \\ 0.0 & 5.0 \end{pmatrix}, \ \boldsymbol{\Sigma}_2 = \begin{pmatrix} 1.0 & -0.25 \\ -0.25 & 0.5 \end{pmatrix}, \ \boldsymbol{\Sigma}_3 = \begin{pmatrix} 1.0 & 0.25 \\ 0.25 & 1.0 \end{pmatrix},$$

and $\tau_1 = 0.5$, $\tau_2 = 0.2$, $\tau_3 = 0$, $\rho_1 = 0$, $\rho_2 = 0.5$, $\rho_3 = 1$. With this dataset we want to show that our model is able to detect whether a behavior is a BRW (behavior 1), a CRW (behavior 3), or a STAP (behavior 2). In the second dataset, we assume $\tau_1 = \tau_2 = \tau_3 = 0.2$, $\rho_1 = 0.2$, $\rho_2 = 0.5$, $\rho_3 = 0.8$, while all the other parameters remain the same. With this dataset, we want to show that we are able to learn the strength of attraction, even when its value is moderate (τ =0.2) and the model is closer to a CRW than a BRW (behavior 3, $\rho = 0.8$). In the last dataset, we have $\tau_1 = \tau_2 = \tau_3 = 0.8$, while all the other parameters are the same as those of the second dataset. With this example, we are interested in showing that, even though the strength of attraction is strong, we can still detect directional persistence. We use the same priors and iterations as Section 3 for the model implementation. We show the simulated datasets in Figure B.1, where we can see that the spatial locations of the 3 behaviors are clearly overlapping.

The posterior estimates of the parameters are shown in Tables B.1, B.2 and B.3, and the parameters that are not well estimated are highlighted in bold. As can be seen, as expected most of the parameters are inside the intervals, and the ones that are not well estimated have intervals that are close to the real values. The posterior probabilities of $K = 3$ are 0.985, 0.969, and 0.98, respectively, for the three datasets. The accuracy of the prediction of z_i, based on the MAP estimator, and the true behavior at time i is 0.942 for the first dataset, 0.916 for the second one, and 0.978 for the third one. Given these results, we can assume that the STAP-HMM parameters can be estimated with the proposed algorithm, which is also able to detect the right number of latent behaviors.

Appendix C Details on the model of McClintock *et al.* (2012). The model is an HMM with a fixed number of behaviors and an emission distribution which is the product of a wrapped Cauchy over the bearing-angle and a Weibull for

	j=1	j=2	j=3
$\hat{\mu}_{j,1}$	-10.007	10.247	0.139
(CI)	(-10.08 -9.937)	(9.602 10.947)	(-60.403 63.725)
$\hat{\mu}_{j,2}$	0.08	9.764	0.645
(CI)	(-0.116 0.273)	(9.246 10.278)	(-60.098 61.962)
$\hat{\eta}_{j,1}$	-0.062	1.157	-2.026
(CI)	(-62.867 62.613)	(0.932 1.301)	(-2.075 -1.978)
$\hat{\eta}_{j,2}$	0.003	1.126	0.022
(CI)	(-61.274 60.611)	(0.076 1.261)	(-0.022 0.068)
$\hat{\tau}_j$	0.502	0.181	0.499
(CI)	(0.495 0.509)	(0.167 0.196)	(0.024 0.975)
$\hat{\rho}_j$	0	0.459	1
(CI)	[0 0)	(0.422 0.493)	(1 1]
$\hat{\mathbf{\Sigma}}_{j,1,1}$	0.482	0.974	0.983
(CI)	(0.451 0.516)	(0.916 1.037)	(0.919 1.054)
$\hat{\mathbf{\Sigma}}_{j,1,2}$	0.02	-0.232	0.267
(CI)	(-0.046 0.088)	(-0.264 -0.201)	(0.22 0.315)
$\hat{\mathbf{\Sigma}}_{j,2,2}$	4.912	0.487	0.991
(CI)	(4.625 5.202)	(0.458 0.518)	(0.931 1.056)
$\hat{\pi}_{1,j}$	0.796	0.101	0.103
(CI)	(0.777 0.815)	(0.087 0.116)	(0.088 0.12)
$\hat{\pi}_{2,j}$	0.085	0.821	0.094
(CI)	(0.073 0.097)	(0.804 0.837)	(0.081 0.107)
$\hat{\pi}_{3,j}$	0.115	0.087	0.799
(CI)	(0.1 0.131)	(0.074 0.101)	(0.78 0.818)
$\hat{\beta}_j$	0.312	0.312	0.308
(CI)	(0.052 0.681)	(0.049 0.676)	(0.049 0.688)
	α	κ	γ
$\hat{}$	0.342	3.46	0.728
(CI)	(0.009 1.347)	(1.184 6.992)	(0.075 2.303)

TABLE B.1

Posterior means and 95% CIs of the parameters of the first simulated dataset for K=3.

the step-length. The temporal evolution of the random variable $z_i^{\text{mc}} \in \{1, 2, \ldots, K^{\text{mc}}\}$ that represents the behavior at time i, follows a first-order Markov process with $z_i^{\text{mc}} | z_{i-1}^{\text{mc}}, \boldsymbol{\pi}_{z_{i-1}^{\text{mc}}}^{\text{mc}} \sim \text{Multinomial}(1, \boldsymbol{\pi}_{z_{i-1}^{\text{mc}}}^{\text{mc}})$. If $z_i^{\text{mc}} = j$, the distributions over the movement-metric are

$$\phi_i | \phi_{i-1}, z_i^{\text{mc}} \sim \text{wCauchy}(\lambda_{i,j}^{\text{mc}}, \epsilon_{i,j}^{\text{mc}}),$$
$$r_i | z_i^{\text{mc}} \sim \text{Weibull}(a_{i,j}^{\text{mc}}, b_{i,j}^{\text{mc}}).$$

If the j-th behavior at time i is a BCRW, we have

$$\lambda_{i,j}^{\text{mc}} = \rho_j^{\text{mc}} \phi_{i-1} + (1 - \rho_j^{\text{mc}}) \zeta_i,$$
$$\epsilon_{i,j}^{\text{mc}} = \text{logit}^{-1}(m_j^{\text{mc}} + g_j^{\text{mc}} \psi_i + q_j^{\text{mc}} \psi_i^2),$$
$$a_{i,j}^{\text{mc}} = a_{1,j}^{\text{mc}} (1 - I_{[0, d_j^{\text{mc}})}(\psi_i)) + a_{2,j}^{\text{mc}} I_{[0, d_j^{\text{mc}})}(\psi_i),$$
$$b_{i,j}^{\text{mc}} = b_{1,j}^{\text{mc}} (1 - I_{[0, d_j^{\text{mc}})}(\psi_i)) + b_{2,j}^{\text{mc}} I_{[0, d_j^{\text{mc}})}(\psi_i),$$

while, if it is a CRW, we obtain $\lambda_{i,j}^{\text{mc}} = \phi_{i-1}$, $\epsilon_{i,j}^{\text{mc}} = \nu_j^{\text{mc}}$, $a_{i,j}^{\text{mc}} = a_j^{\text{mc}}$, $b_{i,j}^{\text{mc}} = b_j^{\text{mc}}$, where ψ_i is the distance between the observation $\mathbf{s}_i$ and the attractor. The prior distributions are: $m_j^{\text{mc}}, g_j^{\text{mc}}, q_j^{\text{mc}} \sim N(0, \tau^{\text{mc}})$, with $\tau^{\text{mc}} \sim G(2, 3)$, $\rho_j^{\text{mc}}, \nu_j^{\text{mc}} \sim U(0, 1)$, $\phi_0 \sim U(0, 2\pi)$, $a_j^{\text{mc}}, a_{1,j}^{\text{mc}}, a_{2,j}^{\text{mc}} \sim U(0, 14000)$, $b_j^{\text{mc}}, b_{1,j}^{\text{mc}}, b_{2,j}^{\text{mc}} \sim U(0, 30)$, $d_j^{\text{mc}} \sim U(0, 14000)$, and $\boldsymbol{\pi}_j^{\text{mc}} \sim \text{Dir}(1, \ldots, 1)$.

Appendix D Turning-angle distribution for different time-intervals. In this section, we want to show that even though a path, at a given time-interval, can

	j=1	j=2	j=3
$\hat{\mu}_{j,1}$	-10.131	10.01	-0.39
(CI)	(-10.495 -9.787)	(9.447 10.578)	(-1.571 0.816)
$\hat{\mu}_{j,2}$	0.556	10	0.743
(CI)	(-0.052 1.152)	(9.517 10.483)	(-0.787 2.062)
$\hat{\eta}_{j,1}$	-0.037	1.088	-2.029
(CI)	(-0.324 0.248)	(0.974 1.205)	(-2.186 -1.895)
$\hat{\eta}_{j,2}$	0.235	1.033	-0.004
(CI)	(-0.037 0.508)	(0.927 1.144)	(-0.062 0.055)
$\hat{\tau}_j$	0.198	0.191	0.196
(CI)	(0.19 0.207)	(0.177 0.207)	(0.142 0.264)
$\hat{\rho}_j$	0.201	0.48	0.795
(CI)	(0.193 0.208)	(0.449 0.511)	(0.741 0.844)
$\hat{\mathbf{\Sigma}}_{j,1,1}$	0.478	0.972	0.959
(CI)	(0.445 0.514)	(0.909 1.039)	(0.886 1.036)
$\hat{\mathbf{\Sigma}}_{j,1,2}$	0.036	-0.241	0.265
(CI)	(-0.034 0.107)	(-0.275 -0.21)	(0.215 0.314)
$\hat{\mathbf{\Sigma}}_{j,2,2}$	4.993	0.492	1.005
(CI)	(4.692 5.301)	(0.462 0.525)	(0.937 1.077)
$\hat{\pi}_{1,j}$	**0.811**	0.096	0.107
(CI)	(0.802 0.818)	(0.081 0.112)	(0.088 0.127)
$\hat{\pi}_{2,j}$	0.084	0.821	0.095
(CI)	(0.071 0.099)	(0.783 0.838)	(0.08 0.111)
$\hat{\pi}_{3,j}$	0.113	0.093	0.794
(CI)	(0.096 0.131)	(0.079 0.11)	(0.771 0.815)
$\hat{\beta}_j$	0.316	0.307	0.311
(CI)	(0.052 0.675)	(0.051 0.672)	(0.049 0.675)
	α	κ	γ
$\hat{}$	0.351	3.382	0.73
(CI)	(0.008 1.419)	(1.143 6.927)	(0.088 2.278)

TABLE B.2

Posterior means and 95% CIs of the parameters of the second simulated dataset for K=3. The parameter whose 95% CI does not contain the true value is shown in bold.

be described by a unimodal and symmetric circular distribution, the distribution over the turning-angle (or bearing-angle) can be asymmetric and multimodal for a greater time-interval.

Let us suppose we have a path $\mathbf{s}^* = (\mathbf{s}^*_{t_1}, \ldots, \mathbf{s}^*_{t_{T^*}})$, where $t_1, \ldots, t_{T^*}$ are equally-spaced temporal-indices, i.e., $t_i - t_{i-1} = t_{i-1} - t_{i-2}$ for all $i = 3, 4, \ldots, T^*$. We assume that the path is a CRW with the following distribution for the step-length and turning-angle:

$$r^*_{t_i} = ||\mathbf{y}^*_{t_i}||_2 \sim \text{Weibull}(a_{\text{sim}}, b_{\text{sim}}), \tag{23}$$
$$\theta^*_{t_i} = \text{atan}^*(y^*_{t_i,2}, y^*_{t_i,1}) \sim \text{wCauchy}(\lambda_{\text{sim}}, \epsilon_{\text{sim}}),$$

where $\mathbf{y}^*_{t_i} = (y^*_{t_i,1}, y^*_{t_i,2})' = R(\phi^*_{t_{i-1}})(\mathbf{s}^*_{t_{i+1}} - \mathbf{s}^*_{t_i})$, $\phi^*_{t_i} = \text{atan}^*(s^*_{t_{i+1},2} - s^*_{t_i,2}, s^*_{t_{i+1},1} - s^*_{t_i,1})$, $\theta^*_{t_i} = \phi^*_{t_i} - \phi^*_{t_{i-1}}$, $\mathbf{s}^*_{t_0} = (-1, 0)'$, and $\mathbf{s}^*_{t_1} = (0, 0)'$. It should be noted that the wrapped-Cauchy is symmetric and unimodal. We assume that the distributions in (23) are the ones that rule the animal's path with a time-step $t_i - t_{i-1}$, but we are only able to observe/record the path at the time-interval $d(t_i - t_{i-1}) = t_{id} - t_{(i-1)d}$ with $d \geq 2$. Hence, we define $\mathbf{s} = (\mathbf{s}_1, \ldots, \mathbf{s}_T)$ as the recorded path with

$$\mathbf{s}_i = \mathbf{s}^*_{t_{id}}. \tag{24}$$

From (24), we can compute the movement metrics, as well as the other sets of coordinates, as explained in Section 2, e.g., $\phi_i = \text{atan}^*(s_{i+1,2} - s_{i,2}, s_{i+1,1} - s_{i,1})$ and $\theta_i = \phi_i - \phi_{i-1}$.

We simulate three paths $\mathbf{s}^*$ (equation (23)) with $T^* = 100\,000$ and the following sets of parameters:

	j=1	j=2	j=3
$\hat{\mu}_{j,1}$	-9.997	10.028	-0.019
(CI)	(-10.057 -9.938)	(9.923 10.137)	(-0.274 0.236)
$\hat{\mu}_{j,2}$	0.054	10.003	0.22
(CI)	(-0.084 0.188)	(9.895 10.113)	(-0.054 0.493)
$\hat{\eta}_{j,1}$	0.01	0.994	-1.977
(CI)	(-0.233 0.254)	(0.908 1.082)	(-2.07 -1.908)
$\hat{\eta}_{j,2}$	0.015	0.962	0.005
(CI)	(-0.244 0.265)	(0.873 1.054)	(-0.049 0.056)
$\hat{\tau}_j$	0.806	0.816	0.915
(CI)	(0.796 0.816)	(0.777 0.862)	(0.77 0.996)
$\hat{\rho}_j$	0.205	0.511	0.824
(CI)	(0.197 0.211)	(0.488 0.537)	(0.791 0.84)
$\hat{\mathbf{\Sigma}}_{j,1,1}$	0.483	0.982	0.975
(CI)	(0.454 0.512)	(0.928 1.04)	(0.917 1.037)
$\hat{\mathbf{\Sigma}}_{j,1,2}$	0.006	-0.244	0.264
(CI)	(-0.06 0.074)	(-0.275 -0.215)	(0.222 0.308)
$\hat{\mathbf{\Sigma}}_{j,2,2}$	4.962	0.495	0.976
(CI)	(4.679 5.259)	(0.468 0.524)	(0.917 1.039)
$\hat{\pi}_{1,j}$	0.799	0.101	0.099
(CI)	(0.781 0.817)	(0.089 0.114)	(0.086 0.114)
$\hat{\pi}_{2,j}$	0.09	**0.817**	0.093
(CI)	(0.079 0.102)	(0.801 0.832)	(0.081 0.105)
$\hat{\pi}_{3,j}$	0.107	0.092	0.801
(CI)	(0.094 0.121)	(0.08 0.105)	(0.783 0.818)
$\hat{\beta}_j$	0.317	0.304	0.31
(CI)	(0.053 0.673)	(0.052 0.675)	(0.047 0.668)
	α	κ	γ
$\hat{}$	0.327	3.377	0.724
(CI)	(0.007 1.279)	(1.16 6.848)	(0.076 2.315)

TABLE B.3

Posterior means and 95% CIs of the parameters of the third simulated dataset for K=3. The parameter whose 95% CI does not contain the true value is shown in bold.

- set1=$\{\lambda_{\text{sim}} = \pi - 0.1, \epsilon_{\text{sim}} = 0.1, a_{\text{sim}} = 1, b_{\text{sim}} = 1\}$;
- set2=$\{\lambda_{\text{sim}} = \pi - 0.35, \epsilon_{\text{sim}} = 0.1, a_{\text{sim}} = 1.7, b_{\text{sim}} = 5\}$;
- set3=$\{\lambda_{\text{sim}} = \pi/4 - 0.2, \epsilon_{\text{sim}} = 0.1, a_{\text{sim}} = 15, b_{\text{sim}} = 10\}$.

We can see the highly concentrated wrapped-Cauchy distributions used to simulate the paths, i.e., the distributions of $\theta^*_{t_i}$, in the first row of Figure D.1. We obtain three datasets of recorded coordinates by assuming $d = 2$ in the first path, while in the second path we assume $d = 3$, and in the third $d = 9$. Using (6) and (8), we derive the samples of the turning-angles θ_i of the recorded paths $\mathbf{s}$ and we evaluate the distributions induced over θ_i with the given time-intervals $t_{id} - t_{(i-1)d}$ by using a kernel estimator; these densities are shown in the second row of Figure D.1. It is clear from the figures that, even though the data at a given time-interval come from a unimodal and symmetric circular distribution, the circular distribution can be bimodal for a greater time-interval (Figure D.1 (d) and (e)) or asymmetric (Figure D.1 (f)). For this reason, a distribution over the circular variable that may be multimodal and asymmetric should be used to describe the data at any time-interval.

Appendix E Sensitivity analysis of the hyper-parameter priors. The number of latent behaviors of the sHDP-HMM depends on the hyper-parameters α, κ and γ, which are random quantities in our model and are assumed to be distributed according to the following priors (see Section 3): $\alpha + \kappa \sim G(0.1, 1)$, $\kappa/(\alpha + \kappa) \sim B(10, 1)$, $\gamma \sim G(0.1, 1)$. In this section, we want to show how the posterior distribution of K changes if we change these priors.

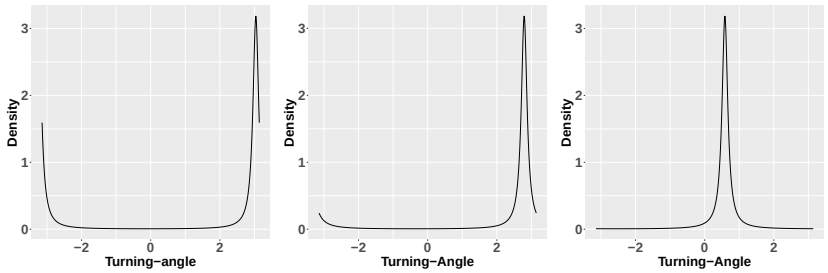

(a) set1 - Wrapped-Cauchy (b) set2 - Wrapped-Cauchy (c) set3 - Wrapped-Cauchy

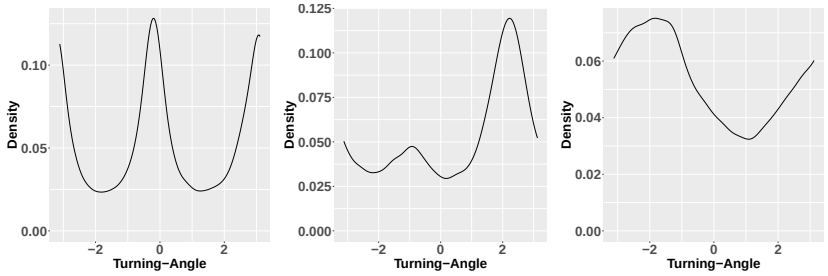

(d) set1 - Kernel density estimate (e) set2 - Kernel density estimate (f) set3 - Kernel density estimate

Fig D.1: The wrapped-Cauchy densities used to simulate the paths $\mathbf{s}^*$ (first row), and the kernel density estimates of the turning-angle distributions of $\mathbf{s}$ (second row).

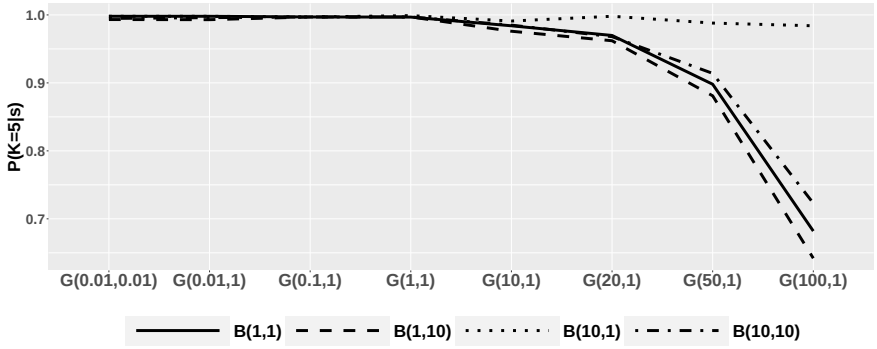

Fig E.1: Values of the posterior probability of the number of behaviors being equal to 5, under 9 Gamma priors for $\alpha + \kappa$ and γ, and 4 Beta priors for $\kappa/(\alpha + \kappa)$.

Parameters $\alpha + \kappa$ and γ can be interpreted in a similar way, since the expected value of the number of behaviors increases with both parameters, while $\kappa/(\alpha + \kappa)$ is the proportion of the extra weight, κ, added to the self transitions, with respect to the total weight, $\alpha + \kappa$; for more details see Fox *et al.* (2011). We estimate different models on the real data, using the same iterations and priors as in Section 3, with the exception of those for $\alpha + \kappa$, $\kappa/(\alpha + \kappa)$, and γ. We assume that $\alpha + \kappa$ and γ have the same prior and we test all the possible combinations of 8 Gamma priors for $\alpha + \kappa$ and γ and 4 Beta priors for $\kappa/(\alpha + \kappa)$, thus obtaining 24 models. In detail, the priors are:

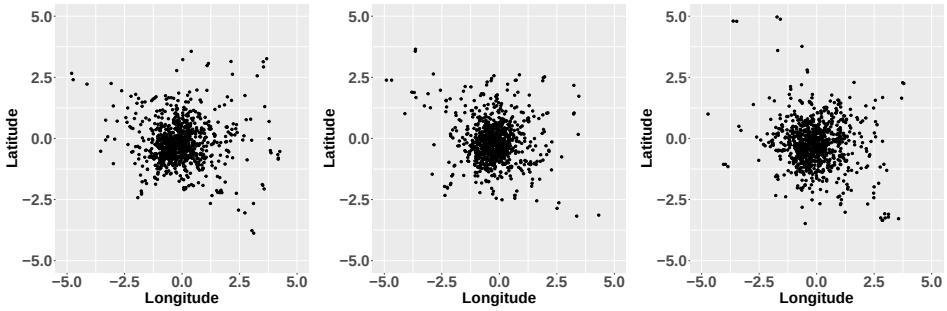

(a) (b) (c)

Fig F.1: Simulated spatial locations using the posterior means of the STAP-HMM as parameters.

- Gamma priors - $G(0.01, 1)$, $G(0.1, 1)$, $G(1, 1)$, $G(10, 1)$, $G(20, 1)$, $G(50, 1)$, $G(100, 1)$, $G(0.01, 0.01)$;
- Beta priors - $B(1, 1)$, $B(10, 1)$, $B(1, 10)$, $B(10, 10)$.

We have a uniform distribution for $\kappa/(\alpha + \kappa)$ ($B(10, 10)$), while the other three have expected values equal to 0.09 ($B(10, 1)$), 0.91 ($B(1, 10)$), 0.5 ($B(10, 10)$), and smaller variances than 0.012. The mean and the variance of 7 out of the 8 Gamma distributions have the same value and are equal to 0.01 ($G(0.01, 1)$), 0.1 ($G(0.1, 1)$), 1 ($G(1, 1)$), 10 ($G(10, 1)$, 20 ($G(20, 1)$, 50 ($G(50, 1)$) and 100 ($G(100, 1)$), while the last one, $G(0.01, 0.01)$, has mean 1 and variance 100. Hence, we have 3 Gamma priors that, a priori, put a greater probability mass on a small number of behaviors ($G(0.01, 1)$, $G(0.1, 1)$, $G(1, 1)$), and 4 priors ($G(10, 1)$, $G(20, 1)$, $G(50, 1)$, $G(100, 1)$) which, a priori, support a high number of behaviors, while $G(0.01, 0.01)$ is often used as a weakly informative prior.

In Figure E.1, we show the posterior probability that the number of latent behaviors is equal to 5 in the 24 models, which is the number found when using the model estimated in Section 3. Since $\mathbb{P}(K = 5|\mathbf{s})$ is always greater than 0.5, $K = 5$ is the number of behaviors with the highest posterior probability for any possible combination of priors, and this is > 0.95 for all the priors, with the exception of $G(50, 1)$ and $G(100, 1)$, where $\mathbb{P}(K = 5|\mathbf{s}) > 0.64$. It is interesting to note that when using the two weakly informative priors $G(0.01, 0.01)$ and $B(1, 1)$, we find that $\mathbb{P}(K = 5|\mathbf{s})$ is approximatively 1. The posterior samples of K have values in $\{5, 6\}$ for the priors $G(0.01, 0.01)$, $G(0.01, 1)$, $G(0.1, 1)$, and $G(1, 1)$, values in $\{5, 6, 7\}$ for the priors $G(10, 1)$ and $G(20, 1)$, and values in $\{5, 6, 7, 8\}$ for the priors $G(50, 1)$ and $G(100, 1)$.

As expected, $\mathbb{P}(K = 5|\mathbf{s})$ tends to decrease if we have a greater prior probability mass on higher values of $\alpha + \kappa$ and γ, and it also increases the number of elements of $\mathbb{N}$ that have a significant posterior probability, that is a measure of the variability of K. The prior on $\kappa/(\alpha+\kappa)$ has a limited impact on $\mathbb{P}(K = 5|\mathbf{s})$ if the distribution over $\alpha+\kappa$ and γ is $G(0.01, 0.01)$, $G(0.01, 1)$, $G(0.1, 1)$, or $G(1, 1)$, and the model with a $B(10, 1)$ prior tends to have the highest $\mathbb{P}(K = 5|\mathbf{s})$ for a given Gamma prior, while a $B(1, 10)$ prior has the smallest. Nonetheless, since $\mathbb{P}(K = 5|\mathbf{s})$ is very large in all of the 24 models, the number of estimated behaviors is always 5, even though we use weakly informative priors ($G(0.01, 0.01)$ and $B(1, 1)$).

Appendix F Real data applications - Simulated trajectories. In order to show that our model can describe the data in Section 3, we show, in Figure F.1, three

		BRW-HMM					CRW-HMM		
		First	Second	Third	Fourth	Fifth	First	Second	Third
STAP-HMM	First	4259	13	1	1	3	4266	9	2
	Second	10	773	7	41	1	8	808	16
	Third	0	27	349	5	0	0	4	377
	Forth	1	31	8	521	0	2	72	487
	Fifth	8	1	1	0	273	2	123	158

TABLE G.1
Two-way table between the MAP behaviors of the STAP-HMM (rows), and the BRW-HMM and CRW-HMM (columns).

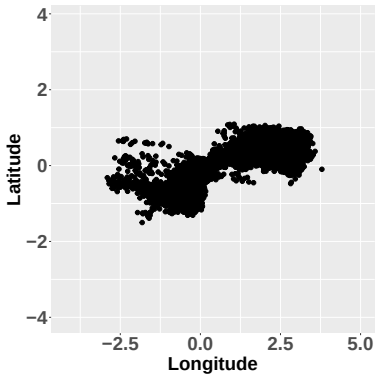

Fig G.1: Observed locations of the sheep.

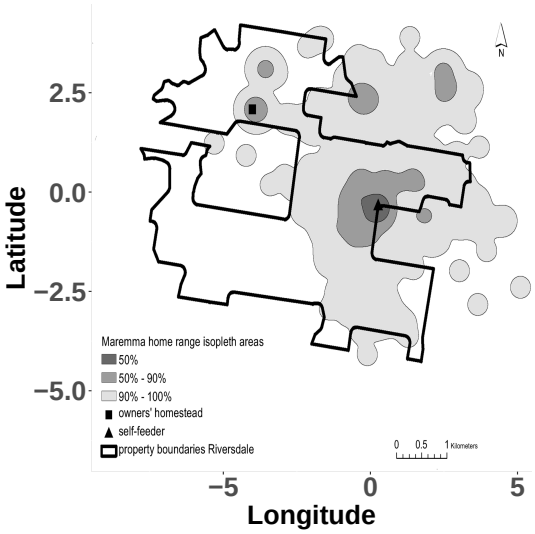

Fig G.2: A copy of the second row of Figure 1 from van Bommel and Johnson (2014), which shows the location of the self-feeder (triangle). The coordinates are not displayed in the original figure and have been added by matching the observed coordinates of all the dogs in the Riversdale property with the home range isopleth.

sets of coordinates obtained by simulating from the STAP-HMM, using the posterior means in Table 2 as parameters. We can clearly see that the simulated data have the central bulk of observations, as well as the extension of the "explored space", as the real data.

	j=1	j=2	j=3	j=4	j=5
$\hat{\mu}_{j,1}$	-3.168	-0.105	17.062	-0.356	0.18
(CI)	(-52.457 43.823)	(-22.525 23.693)	(-15.255 59.094)	(-0.423 -0.295)	(0.17 0.19)
$\hat{\mu}_{j,2}$	-0.294	3.153	5.021	-0.314	-0.404
(CI)	(-46.638 45.392)	(-7.564 31.502)	(-25.564 41.621)	(-0.389 -0.244)	(-0.412 -0.395)
$\hat{\tau}_j$	0	0.008	0.008	0.624	0.985
(CI)	(0 0)	(0 0.02)	(0 0.038)	(0.572 0.681)	(0.974 0.996)
$\hat{\mathbf{\Sigma}}_{j,1,1}$	0.001	0.035	0.854	0.12	0.006
(CI)	(0.001 0.001)	(0.025 0.05)	(0.709 1.062)	(0.097 0.15)	(0.005 0.007)
$\hat{\mathbf{\Sigma}}_{j,1,2}$	0	-0.002	-0.083	0.031	0.001
(CI)	(0 0)	(-0.005 0.001)	(-0.155 -0.023)	(0.015 0.047)	(0 0.002)
$\hat{\mathbf{\Sigma}}_{j,2,2}$	0.001	0.019	0.427	0.164	0.005
(CI)	(0.001 0.001)	(0.014 0.027)	(0.357 0.522)	(0.134 0.204)	(0.004 0.006)
$\hat{\pi}_{1,j}$	0.847	0.077	0.023	0.042	0.011
(CI)	(0.834 0.86)	(0.066 0.089)	(0.015 0.031)	(0.032 0.052)	(0.005 0.019)
$\hat{\pi}_{2,j}$	0.28	0.396	0.143	0.085	0.096
(CI)	(0.236 0.33)	(0.338 0.458)	(0.102 0.185)	(0.048 0.125)	(0.067 0.126)
$\hat{\pi}_{3,j}$	0.07	0.209	0.504	0.161	0.056
(CI)	(0.039 0.107)	(0.148 0.276)	(0.429 0.571)	(0.11 0.217)	(0.026 0.093)
$\hat{\pi}_{4,j}$	0.17	0.19	0	0.447	0.193
(CI)	(0.125 0.22)	(0.123 0.262)	(0 0.006)	(0.359 0.526)	(0.151 0.24)
$\hat{\pi}_{5,j}$	0.883	0	0.004	0.003	0.11
(CI)	(0.777 0.979)	(0 0.003)	(0 0.029)	(0 0.026)	(0.017 0.212)
$\hat{\beta}_j$	0.25	0.174	0.122	0.178	0.223
(CI)	(0.074 0.48)	(0.04 0.373)	(0.016 0.308)	(0.042 0.386)	(0.068 0.44)
	α	κ	γ		
$\hat{}$	0.266	2.613	1.204		
(CI)	(0.007 1.008)	(1.338 4.357)	(0.296 2.904)		

TABLE G.2
Posterior means and 95% CIs of the BRW-HMM parameters for K=5.

	j=1	j=2	j=3
$\hat{\eta}_{j,1}$	-0.005	-0.044	0.026
(CI)	(-0.006 -0.004)	(-0.059 -0.029)	(-0.021 0.073)
$\hat{\eta}_{j,2}$	0	0.001	-0.008
(CI)	(-0.001 0.001)	(-0.009 0.011)	(-0.046 0.029)
$\hat{\mathbf{\Sigma}}_{j,1,1}$	0.001	0.036	0.597
(CI)	(0.001 0.001)	(0.029 0.045)	(0.541 0.657)
$\hat{\mathbf{\Sigma}}_{j,1,2}$	0	0	0.013
(CI)	(0 0)	(-0.002 0.002)	(-0.017 0.042)
$\hat{\mathbf{\Sigma}}_{j,2,2}$	0.001	0.018	0.394
(CI)	(0.001 0.001)	(0.015 0.022)	(0.357 0.435)
$\hat{\pi}_{1,j}$	0.849	0.086	0.064
(CI)	(0.837 0.861)	(0.074 0.099)	(0.055 0.075)
$\hat{\pi}_{2,j}$	0.349	0.415	0.236
(CI)	(0.308 0.394)	(0.364 0.463)	(0.198 0.274)
$\hat{\pi}_{3v}$	0.245	0.213	0.542
(CI)	(0.213 0.279)	(0.168 0.256)	(0.501 0.583)
$\hat{\beta}_j$	0.321	0.3	0.303
(CI)	(0.047 0.696)	(0.047 0.675)	(0.046 0.671)
	α	κ	γ
$\hat{}$	0.229	2.175	0.765
(CI)	(0.005 0.907)	(0.778 4.439)	(0.088 2.343)

TABLE G.3
Posterior means and 95% CIs of the CRW-HMM parameters for K=3.

Appendix G Real data applications - CRW-HMM and BRW-HMM. In this Appendix, we show the results obtained when an HMM that can only estimate CRWs (CRW-HMM) or BRWs (BRW-HMM) is considered. The priors, iterations,

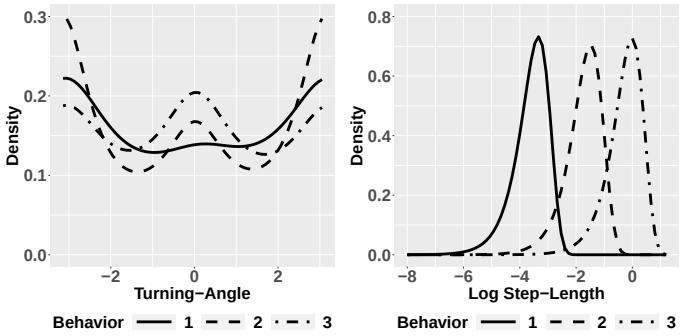

(a) (b)

Fig G.3: Turning-angle (a) and log step-length (b) predictive distributions for the CRW-HMM behaviors.

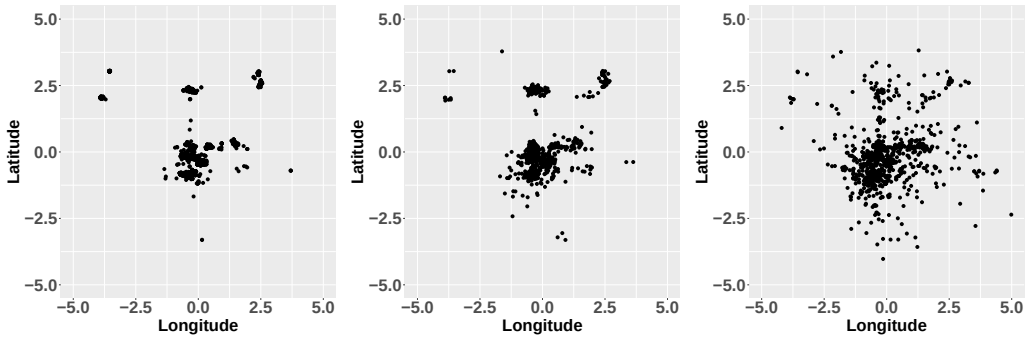

(a) First behavior (b) Second behavior (c) Third behavior

Fig G.4: Spatial locations of the MAP behavior for the CRW-HMM model.

burnin and thin are the same as those used to obtain posterior samples of the STAP-HMM. After fitting the model, we found that the number of estimated behaviors is 5 (with probability 0.99) for the BRW-HMM, and 3 (with probability 0.98) for the CRW-HMM. The posterior means and CIs of all the parameters are shown in Tables G.2 and G.3. We indicate the j-th behavior for the BRW-HMM and CRW-HMM, respectively, as $\text{LB}_{j,\text{BRW}}$ and $\text{LB}_{j,\text{CRW}}$.

BRW-HMM. It is clear, from Table G.1, that the MAP behaviors of the STAP-HMM and BRW-HMM have the same temporal dynamics, i.e., the animal exhibits behavior LB_j and $\text{LB}_{j,\text{BRW}}$ at the same temporal points. This almost one-to-one relation explains why the parameters estimated for LB_4 and LB_5, i.e., the BRW-type behaviors of our proposal, are very similar to $\text{LB}_{4,\text{BRW}}$ and $\text{LB}_{5,\text{BRW}}$, respectively (see Tables 2 and G.2). As the behaviors have the same temporal evolution as the STAP-HMM, they have the same spatial locations and time of the day when they are more likely to be observed. This means that the interpretation is similar, but the BRW-HMM fails to recognize the directional persistence that is present in the first and second behaviors, and estimates RWs, i.e., $\hat{\tau}_1 = 0$ and $\hat{\tau}_2 = 0.008$, respectively.

CRW-HMM. As can be seen from Table G.1, the dog follows LB_1 and $\text{LB}_{1,\text{CRW}}$ at the same temporal points, which is also shown by the spatial locations of $\text{LB}_{1,\text{CRW}}$ that can be seen in Figure G.4 (a). The posterior estimates of the likelihood parameters of LB_1 and $\text{LB}_{1,\text{CRW}}$ are almost identical, and this can also be verified from the posterior

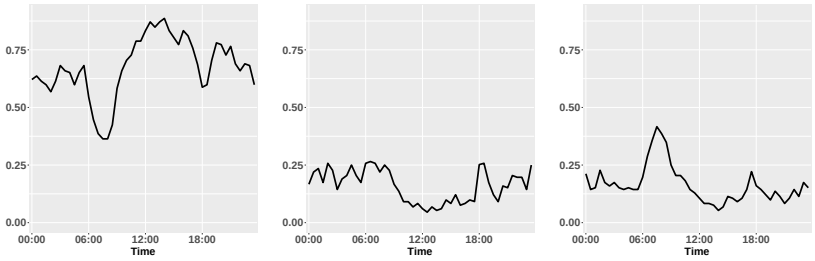

(a) First behavior (b) Second behavior (c) Third behavior

Fig G.5: The values of the lines at each time (x-axis) represent the proportion of times that the CRW-HMM MAP behaviors are observed (y-axis).

densities in Figure G.3. $\text{LB}_{2,\text{CRW}}$ generally has the same temporal indices as LB_2, similar spatial locations (Figure G.4 (a)), similar frequencies during the day (Figure G.5 (b)), a similar step-length distribution (Figure G.3 (b)), but a different circular one (Figure G.3 (d)). This behavior has a higher speed than $\text{LB}_{1,CRW}$, and a bimodal circular distribution with the major mode at $-\pi$, and a smaller one at 0. $\text{LB}_{3,CRW}$ has the highest speed and a circular distribution with two modes, at 0 and $-\pi$, which have approximatively the same density (see Figure G.3), and are more likely during the night or in the early hours of the morning.

General comments. Our proposal is able to estimate behaviors that are similar, in interpretation and posterior inference, to $\text{LB}_{4,\text{BRW}}$, $\text{LB}_{5,\text{BRW}}$ and $\text{LB}_{1,\text{CRW}}$, as well as to find two behaviors, LB_2 and LB_3, that are not estimated by the other two models. The CRW-HMM finds 3 behaviors but, since none of them has a spatial distribution concentrated on the livestock paddock (Figure G.1) as LB_4, it does not identify when the dog is attending the livestock. The BRW-HMM fails to find any structure in $\text{LB}_{1,\text{BRW}}$ or in $\text{LB}_{2,\text{BRW}}$, where it estimates a simple RW.

REFERENCES

Abe, T. and Ley, C. (2017). A tractable, parsimonious and flexible model for cylindrical data, with applications. *Econometrics and Statistics*, **4**, 91–104.

Anderson, C. R. and Lindzey, F. G. (2003). Estimating cougar predation rates from gps location clusters. *The Journal of Wildlife Management*, **67**(2), 307–316.

Barton, K. A., Phillips, B. L., Morales, J. M., and Travis, J. M. J. (2009). The evolution of an 'intelligent' dispersal strategy: biased, correlated random walks in patchy landscapes. *Oikos*, **118**(2), 309–319.

Bezanson, J., Edelman, A., Karpinski, S., and Shah, V. B. (2017). Julia: A fresh approach to numerical computing. *SIAM review*, **59**(1), 65–98.

Biernacki, C., Celeux, G., and Govaert, G. (2000). Assessing a mixture model for clustering with the integrated completed likelihood. *IEEE Trans. Pattern Anal. Mach. Intell.*, **22**(7), 719–725.

Blackwell, P. (1997). Random diffusion models for animal movement. *Ecological Modelling*, **100**(1), 87 – 102.

Brook, L. A., Johnson, C. N., and Ritchie, E. G. (2012). Effects of predator control on behaviour of an apex predator and indirect consequences for mesopredator suppression. *Journal of Applied Ecology*, **49**(6), 1278–1286.

Brost, B. M., Hooten, M. B., Hanks, E. M., and Small, R. J. (2015). Animal movement constraints improve resource selection inference in the presence of telemetry error. *Ecology*, **96**(10), 2590–2597.

Buderman, F. E., Hooten, M. B., Ivan, J. S., and Shenk, T. M. (2018a). Large-scale movement behavior in a reintroduced predator population. *Ecography*, **41**(1), 126–139.

Buderman, F. E., Hooten, M. B., Alldredge, M. W., Hanks, E. M., and Ivan, J. S. (2018b). Time-varying predatory behavior is primary predictor of fine-scale movement of wildland-urban cougars. *Movement Ecology*, **6**(1), 22.

Cagnacci, F., Boitani, L., Powell, R. A., and Boyce, M. S. (2010). Animal ecology meets gps-based radiotelemetry: a perfect storm of opportunities and challenges. *Philosophical Transactions of the Royal Society of London B: Biological Sciences*, **365**(1550), 2157–2162.

Celeux, G., Forbes, F., Robert, C. P., Titterington, D. M., Futurs, I., and Rhône-alpes, I. (2006). Deviance information criteria for missing data models. *Bayesian Analysis*, **4**, 651–674.

Christ, A., Hoef, J. V., and Zimmerman, D. L. (2008). An animal movement model incorporating home range and habitat selection. *Environmental and Ecological Statistics*, **15**(1), 27–38.

Codling, E. and Hill, N. (2005). Sampling rate effects on measurements of correlated and biased random walks. *Journal of Theoretical Biology*, **233**(4), 573 – 588.

Codling, E. A., Plank, M. J., and Benhamou, S. (2008). Random walk models in biology. *Journal of The Royal Society Interface*, **5**(25), 813–834.

Dunn, J. E. and Gipson, P. S. (1977). Analysis of radiotelemetry data in studies of home range. *Biometrics*, **33**(1).

Fleming, C. H., Calabrese, J. M., Mueller, T., Olson, K. A., Leimgruber, P., and Fagan, W. F. (2014). Non-markovian maximum likelihood estimation of autocorrelated movement processes. *Methods in Ecology and Evolution*, **5**(5), 462–472.

Fortin, D., Morales, J. M., and Boyce, M. S. (2005). Elk winter foraging at fine scale in yellowstone national park. *Oecologia*, **145**(2), 334–342.

Fox, E. B., Sudderth, E. B., Jordan, M. I., and Willsky, A. S. (2011). A sticky hdp-hmm with application to speaker diarization. *The Annals of Applied Statistics*, **5**(2A), 1020–1056.

Frair, J. L., Fieberg, J., Hebblewhite, M., Cagnacci, F., DeCesare, N. J., and Pedrotti, L. (2010). Resolving issues of imprecise and habitat-biased locations in ecological analyses using gps telemetry data. *Philosophical Transactions of the Royal Society of London B: Biological Sciences*, **365**(1550), 2187–2200.

Friendly, M., Monette, G., and Fox, J. (2013). Elliptical insights: Understanding statistical methods through elliptical geometry. *Statistical Science*, **28**(1), 1–39.

Frühwirth-Schnatter, S. and Malsiner-Walli, G. (2019). From here to infinity: sparse finite versus dirichlet process mixtures in model-based clustering. *Advances in Data Analysis and Classification*, **13**(1), 33–64.

Fryxell, J. M., Hazell, M., Börger, L., Dalziel, B. D., Haydon, D. T., Morales, J. M., McIntosh, T., and Rosatte, R. C. (2008). Multiple movement modes by large herbivores at multiple spatiotemporal scales. *Proceedings of the National Academy of Sciences*, **105**(49), 19114–19119.

Gehring, T. M., VerCauteren, K. C., and Cellar, A. C. (2017). Good fences make good neighbors: Implementation of electric fencing for establishing effective livestock-protection dogs. *Human-Wildlife Interactions*, **5**(1), 106–111.

Gelman, A., Robert, C., Chopin, N., and Rousseau, J. (1995). Bayesian data analysis.

Hanks, E. M., Hooten, M. B., and Alldredge, M. W. (2015). Continuous-time discrete-space models for animal movement. *Annals of Applied Statistics*, **9**(1), 145–165.

Harris, K. J. and Blackwell, P. G. (2013). Flexible continuous-time modelling for heterogeneous animal movement. *Ecological Modelling*, **255**, 29 – 37.

Hastie, D. I. and Green, P. J. (2012). Model choice using reversible jump markov chain monte carlo. *Statistica Neerlandica*, **66**(3), 309–338.

Hebblewhite, M. and Merrill, E. (2008). Modelling wildlife and uman relationships for social species with mixed-effects resource selection models. *Journal of Applied Ecology*, **45**(3), 834–844.

Hooten, M., Johnson, D., McClintock, B., and Morales, J. (2017). *Animal Movement: Statistical Models for Telemetry Data*. CRC Press.

Ishwaran, H. and Zarepour, M. (2002). Exact and approximate sum representations for the Dirichlet process. *Canadian Journal of Statistics*, **30**(2), 269–283.

Jammalamadaka, S. R. and Kozubowski, T. J. (2004). New families of wrapped distributions for modeling skew circular data. *Communications in Statistics - Theory and Methods*, **33**(9), 2059–2074.

Johnson, D. S., London, J. M., Lea, M.-A., and Durban, J. W. (2008). Continuous-time correlated random walk model for animal telemetry data. *Ecology*, **89**(5), 1208–1215.

Johnson, D. S., Hooten, M. B., and Kuhn, C. E. (2013). Estimating animal resource selection from telemetry data using point process models. *Journal of Animal Ecology*, **82**(6), 1155–1164.

Jonsen, I. D., Flemming, J. M., and Myers, R. A. (2005). Robust state-space modeling of animal movement data. *Ecology*, **86**(11), 2874–2880.

Langrock, R., King, R., Matthiopoulos, J., Thomas, L., Fortin, D., and Morales, J. M. (2012). Flexible and practical modeling of animal telemetry data: hidden Markov models and extensions. *Ecology*, **93**(11), 2336–2342.

Langrock, R., Hopcraft, G., Blackwell, P., Goodall, V., King, R., Niu, M., Patterson, T., Pedersen, M., Skarin, A., and Schick, R. (2014). Modelling group dynamic animal movement. *Methods in Ecology and Evolution*, **5**(2), 190–199.

Mastrantonio, G. (2018). The joint projected normal and skew-normal: A distribution for poly-cylindrical data. *Journal of Multivariate Analysis*, **165**, 14 – 26.

Mastrantonio, G., Maruotti, A., and Jona Lasinio, G. (2015). Bayesian hidden Markov modelling using circular-linear general projected normal distribution. *Environmetrics*, **26**, 145–158.

Mastrantonio, G., Jona Lasinio, G., and Gelfand, A. E. (2016). Spatio-temporal circular models with non-separable covariance structure. *TEST*, **23**, 331–350.

Mastrantonio, G., Grazian, C., Mancinelli, S., and Bibbona, E. (2019). New formulation of the logistic-gaussian process to analyze trajectory tracking data. *Ann. Appl. Stat.*, **13**(4), 2483–2508.

McClintock, B. T. and Michelot, T. (2018). momentuhmm: R package for generalized hidden markov models of animal movement. *Methods in Ecology and Evolution*, **9**(6), 1518–1530.

McClintock, B. T., King, R., Thomas, L., Matthiopoulos, J., McConnell, B. J., and Morales, J. M. (2012). A general discrete-time modeling framework for animal movement using multistate random walks. *Ecological Monographs*, **82**(3), 335–349.

McClintock, B. T., Johnson, D. S., Hooten, M. B., Ver Hoef, J. M., and Morales, J. M. (2014). When to be discrete: the importance of time formulation in understanding animal movement. *Movement Ecology*, **2**(1), 21.

McGrew, J. C. and Blakesley, C. S. (1982). How komondor dogs reduce sheep losses to coyotes. *Journal of Range Management*, **6**(35), 693–696.

Merrill, S. B. and David Mech, L. (2000). Details of extensive movements by minnesota wolves (canis lupus). *The American Midland Naturalist*, **144**(2), 428–433.

Michelot, T. and Blackwell, P. G. (2019). State-switching continuous-time correlated random walks. *Methods in Ecology and Evolution*, **10**(5), 637–649.

Michelot, T., Langrock, R., and Patterson, T. A. (2016). movehmm: an r package for the statistical modelling of animal movement data using hidden markov models. *Methods in Ecology and Evolution*, **7**(11), 1308–1315.

Morales, J. M. and Ellner, S. P. (2002). Scaling up animal movements in heterogeneous landscapes: the importance of behavior. *Ecology*, **83**(8), 2240–2247.

Morales, J. M., Haydon, D. T., Frair, J., Holsinger, K. E., and Fryxell, J. M. (2004). Extracting more out of relocation data: building movement models as mixtures of random walks. *Ecology*, **85**(9), 2436–2445.

Nathan, R., Getz, W. M., Revilla, E., Holyoak, M., Kadmon, R., Saltz, D., and Smouse, P. E. (2008). A movement ecology paradigm for unifying organismal movement research. *Proceedings of the National Academy of Sciences*, **105**(49), 19052–19059.

Parton, A. and Blackwell, P. G. (2017). Bayesian inference for multistate 'step and turn' animal movement in continuous time. *Journal of Agricultural, Biological and Environmental Statistics*, **22**(3), 373–392.

Patterson, T., Thomas, L., Wilcox, C., Ovaskainen, O., and Matthiopoulos, J. (2008). State-space models of individual animal movement. *Trends in Ecology & Evolution*, **23**(2), 87–94.

Patterson, T. A., Parton, A., Langrock, R., Blackwell, P. G., Thomas, L., and King, R. (2017). Statistical modelling of individual animal movement: an overview of key methods and a discussion of practical challenges. *AStA Advances in Statistical Analysis*, **101**(4), 399–438.

Pohle, J., Langrock, R., van Beest, F. M., and Schmidt, N. M. (2017). Selecting the number of states in hidden markov models: Pragmatic solutions illustrated using animal movement. *Journal of Agricultural, Biological and Environmental Statistics*, **22**(3), 270–293.

Rivest, L.-P., Duchesne, T., Nicosia, A., and Fortin, D. (2016). A general angular regression model for the analysis of data on animal movement in ecology. *Journal of the Royal Statistical Society: Series C (Applied Statistics)*, **65**(3), 445–463.

Schultz, C. B. and Crone, E. E. (2001). Edge-mediated dispersal behavior in a prairie butterfly. *Ecology*, **82**(7), 1879–1892.

van, Bommel, L. and Johnson, C. (2014). Data from: Where do livestock guardian dogs go? movement patterns of free-ranging maremma sheepdogs, doi:10.5441/001/1.pv048q7v.

van Bommel, L. and Invasive Animals Cooperative Research Centre (2010). *Guardian Dogs: Best Practice Manual for the Use of Livestock Guardian Dogs*. Invasive Animals Cooperative Research Centre.

van Bommel, L. and Johnson, C. N. (2012). Good dog! using livestock guardian dogs to protect livestock from predators in australia's extensive grazing systems. *Wildlife Research*, **39**(3), 220–229.

van Bommel, L. and Johnson, C. N. (2014). Where do livestock guardian dogs go? movement patterns of free-ranging maremma sheepdogs. *PLOS ONE*, **9**(10), 1–12.

van Bommel, L. and Johnson, C. N. (2016). Livestock guardian dogs as surrogate top predators? how maremma sheepdogs affect a wildlife community. *Ecology and Evolution*, **6**(18), 6702–6711.

Volant, S., Bérard, C., Martin-Magniette, M.-L., and Robin, S. (2014). Hidden markov models with mixtures as emission distributions. *Statistics and Computing*, **24**(4), 493–504.

Walton, Z., Samelius, G., Odden, M., and Willebrand, T. (2017). Variation in home range size of red foxes vulpes vulpes along a gradient of productivity and human landscape alteration. *PLOS ONE*, **12**(4), 1–14.

Wang, F. and Gelfand, A. E. (2013). Directional data analysis under the general projected normal distribution. *Statistical Methodology*, **10**(1), 113–127.